DESIGN AND SHAPE OPTIMIZATION OF UNMANNED, SEMI-RIGID AIRSHIP FOR RAPID DESCENT USING HYBRID GENETIC ALGORITHM

A Thesis Submitted to

the Faculty of Graduate and Postdoctoral Studies

by

Vinay Singh, B.E.

In Partial Fulfillment of the Requirements for the Degree of

MASTER OF APPLIED SCIENCE

in Mechanical Engineering

Ottawa-Carleton Institute for Mechanical and Aerospace Engineering

University of Ottawa

Ottawa, Canada

Acknowledgements

I would like to express my profound gratitude to Professor Dr. Eric Lanteigne for his patient guidance, enthusiastic encouragement and useful critiques pertinent to the research work. His advice and assistance have been key in keeping my progress on schedule. I would like to extend my gratitude to Mr. Ahmad Alsayed for his constructive recommendations and valuable support throughout the program.

Finally, I would like to give my special thanks to my parents and my sisters- Sunita and Nikita for their support and encouragement during the studies.

Abstract

Singh, Vinay. M.A.Sc. University of Ottawa, August 2018. *Design and shape optimization of unmanned, semi-rigid airship for rapid descent using hybrid genetic algorithm* . Supervised by Dr. E. Lanteigne, Ph.D..

Airships provide an eco-friendly and cost-effective means to suit sustained airborne operations. Smaller autonomous airships are highly susceptible to adverse atmospheric conditions owing to their under-actuated, underpowered and bulky size relative to other types of unmanned aerial vehicles (UAVs). To mitigate these limitations, careful considerations of the size and shape must be made at the design stage. This research presents a methodology for obtaining an optimized shape of a semi-rigid airship. Rapid descent of the LTA ship is achieved by means of a moving gondola attached to a rigid keel mounted under the helium envelope from the bow to the mid-section of the hull. The study entails the application of a robust hybrid genetic algorithm (HGA) for the multi-disciplinary design and optimization of an airship capable of rapid descent, with lower drag and optimum surface area. A comprehensive sensitivity analysis was also performed on the basis of algorithmic parameters and atmospheric conditions. With the help of HGA, a semi-rigid airship capable of carrying a payload of 0.25 kg to 1.0 kg and capable of pitching at right angles is conceptually designed. The algorithm is also tested on commercially available vehicles to validate the results. In multi-objective optimization problems (MOOPs), the significance of different objectives is dependent on the user.

Keywords: genetic algorithm, hill climbing, optimization, Pareto optimality, rapid descent, semi-rigid airship

Table of Contents

Abstract iii

List of Tables vi

List of Figures vii

List of Symbols ix

List of Acronyms xii

Chapter 1. Introduction 1
- 1.1. Motivation 1
- 1.2. Problem description 4
- 1.3. Thesis layout 7

Chapter 2. Literature review 8
- 2.1. Airship shape optimization 8
- 2.2. Optimization methods 14
- 2.3. GA in detail 18
- 2.4. Pareto optimality 24

Chapter 3. Modelling and theory 27
- 3.1. Modelling of the airship 27
  - 3.1.1. Weight 28
  - 3.1.2. Altitude 29
  - 3.1.3. Speed 30
  - 3.1.4. Aerodynamics 31
  - 3.1.5. Material 33
  - 3.1.6. Structure 34
  - 3.1.7. Envelope stress 36
  - 3.1.8. Surface Area 36
  - 3.1.9. Relation between buoyancy and gross weight 36
  - 3.1.10. Centre of gravity 37

Chapter 4. Optimization set up 38
- 4.1. Formulation of the multi-objective function 38
- 4.2. Optimization approach 39
- 4.3. Implementation details of the algorithm 41
  - 4.3.1. Encoding, precision, and limits 42
  - 4.3.2. Initial population - a set of feasible solutions 43
  - 4.3.3. Natural Selection 43
  - 4.3.4. Pairing 43

4.3.5. Crossover 44
4.3.6. Mutation 46
4.3.7. Hill climbing 46
4.3.8. Convergence criteria 47
4.4. Benchmarking the algorithm 48
4.5. Optimization engine- Pareto GA 49

Chapter 5. Simulation results and discussion 53
5.1. Results 53
5.1.1. Optimization model variants 55
5.2. Sensitivity analysis 59
5.3. Tests for various payload capacities 63
5.4. Confirmation to a commercial product 65
5.4.1. Example 1 65
5.4.2. Example 2 66

Chapter 6. Conclusion 69
6.1. Key findings 69
6.2. Future work 70

References 71

Appendix A. Appendix: Important concepts 76

List of Tables

Table 4.1. Input Parameters 41
Table 4.2. Rank Weighting 44
Table 4.3. HGA Input Parameters 48
Table 4.4. Benchmark test results for the HGA 49

Table 5.1. Input Parameters 54
Table 5.2. Comparison of design properties for different profiles 57
Table 5.3. Comparison of characteristics for various payload configuration 64
Table 5.4. Comparison of different semi-rigid airships properties 67

List of Figures

Figure 1.1. Modern unmanned airships: (a) Aurora airship AS 800 [8], (b) Airship deploying UAS [9], (c) High altitude airship Berkut [10], (d) SAIC Skybus 80K [9]) 2
Figure 1.2. Structural modelling of semi-rigid airship: Old airship vs. new airship 3
Figure 1.3. Airship descent using CG control [12] 4
Figure 1.4. Airship gondola prototype [12] 5
Figure 1.5. Airship axes configuration [11] 6

Figure 2.1. Modelling of flow field and geometry of body profile [16] 9
Figure 2.2. Modelling of geometry of body profile 12
Figure 2.3. Forces on tether elements with respect to confluence point [22] 13
Figure 2.4. Change in operational height due to blow-by [22] 13
Figure 2.5. Optimization flowchart [26] 15
Figure 2.6. Optimization methods [25] 16
Figure 2.7. GA operators 19
Figure 2.8. Pareto optimality [36] 24
Figure 2.9. Design space [39] 25
Figure 2.10. Criterion space [39] 26

Figure 3.1. Structural modelling of semi-rigid airship: Old airship vs. new airship 34
Figure 3.2. Airship body profile for the current design 35

Figure 4.1. Design methodology flowchart 40
Figure 4.2. GA flowchart 45
Figure 4.3. Hill climbing flowchart 47
Figure 4.4. Design space of Rastrigin's function 48
Figure 4.5. Pareto GA flowchart [29] 51
Figure 4.6. Final population distribution 52

Figure 5.1. Fitness trend 54
Figure 5.2. Body profile comparison with different weights 56
Figure 5.3. Improvement in the design with respect to reference design 58
Figure 5.4. Mass distribution 59
Figure 5.5. Volume vs. Payload plot 60
Figure 5.6. Fitness vs 'a' 60
Figure 5.7. Fitness vs 'b' 61
Figure 5.8. Fitness vs 'c' 61
Figure 5.9. Fitness vs 'd' 62
Figure 5.10. Fitness Vs. GA Operators 63

Figure 5.11. Simulation for various payload capacities 64
Figure 5.12. Commercially available RC airship 66
Figure 5.13. Simulation for various payload capacities [5] 67

Figure 6.1. Airship body profile for future contributions 70

List of Symbols

P_{cr}	Propulsive power for cruise	8
D	Diameter	8
V_{cr}	Cruise velocity	8
η_{prop}	Propulsive efficiency	8
e^n	Transition method	8
C_D	Drag coefficient	10
r_0	Radius of body of revolution	10
θ	Momentum thickness	10
U_e^*	Velocity at the edge of the boundary layer	10
S	Surface area at maximum radius	30
A	Area factor	10
H	Shape factor	10
C_{DV}	Volumetric drag coefficient	11
l	Length of airship	11
d	Maximum diameter of airship	11
Re	Reynold's number	11
ρ_a	Density of air	11
ν	Velocity of air	11
μ	Dynamic viscosity of air	11
y	Objective function matrix	17
λ	Lagrange multipliers	17
ϕ	Constraints matrix	17
N_{keep}	Number of individuals retained in GA	20
mg	Vector containing pairing rows	37
P_n	Cumulative probability of the population pool	21
β	Mixing parameter	22

T	Temperature at certain height	30
T_0	Temperature at sea level	30
L	Temperature lapse rate	30
h	Height above the sea level	30
g	Gravitational acceleration	30
M	Molar mass	30
P	Pressure	30
R	Ideal (universal) gas constant	30
P_i	Power needed by airship	30
S	Flight speed of an airship	30
N	Number of grid points in CFD analysis	32
C_f	Coefficient of form drag	32
a, b, c, d	Design variables of the airship hull shape	35
α	Angle of extension of keel	35
F	Fitness or objective function	38
SA	Surface area	38
κ	Kappa	38
B	Buoyancy	38
W	Total weight of the airship	38
w_i	Weight constants	38
m_t	Total mass of the airship	36
m_e	Mass of envelope	37
m_{gas}	Mass of gas	37
m_g	Mass of gondola	37
m_b	Mass of ballast	37
ρ_{gas}	Mass of helium gas	37
V	Volume of airship	37
m_r	Mass of rail	38
m_{ru}	Mass of rail per unit length	41
ρ_{fab}	Density of envelope	41

x_0 Design vector 42
N_i Number of individuals in the population 43

List of Acronyms

CV	Center of volume 4
CG	Center of gravity 3
CB	Center of buoyancy 5
CFD	Computational fluid dynamics 10
RSM	Response surface methodology 11
MDO	Multi-disciplinary optimization 12
SA	Surface area 12
PSO	Particle Swarm Optimization 14
GA	Genetic algorithm 18
CPU	Central processing unit 19
HGA	Hybrid Genetic algorithm 23
HC	Hill climbing 23
UAS	Unmanned aircraft system 27
RPV	Remotely piloted vehicle 27
RC	Radio controlled 27
HTA	Heavier-than-air 29
SL	Sea level 30
LTA	Lighter-than-air 34
UV	Ultra-violet 33
MOOP	Multi-objective optimization 38
MA	Memetic algorithm 41

Chapter 1

Introduction

An airship or dirigible is a type of aircraft that uses lighter-than-air gas to gain lift and it navigates through the air under its power [1]. Typically classified into rigid, semi-rigid and non-rigid airship, the focus of the present work is the second type. There are four basic components of a miniature semi-rigid airship, which also happens to be subject of discussion- hull, tail unit (optional), gondola and keel.

1.1 Motivation

Airships use lighter than air gases like hydrogen or helium to gain buoyancy necessary for lift. Invented by the French engineer Henri Giffard in the year 1852 [2], airships have seen significant changes in the design since their inception. With the technological advances in heavier-than-air aircraft as well as accidents owing to flammable hydrogen, came a sharp decline in the development and use of airships. However, in the past decade or so, there has been renewed research interest in these aircrafts. Hydrogen is replaced by safer and almost equally light helium. On account of which, airships offer longer endurance flights at speeds as high as 100 km/h [3]. Airships are tailored for applications such as: payload delivery, prolonged aerial surveillance, photography, advertizing and so on [4]. Owing to their safe, user-friendly and cost-effective qualities, airships have leverage over heavier-than-air vehicles like rotary wing aircraft or any ground vehicle. Airships are most commonly classified on the basis of structural configuration: rigid airships, semi-rigid airships and non-rigid airships [5]. Rigid airships (e.g. Hindenburg) are made up of solid shell framework with one or more gas cells [6]. These maintain their shape by virtue of their framework and not from the pressure of the lifting gas. Semi-rigid airships have a partial rigid frame mounted inside or outside to subside the total load carried by the airship. Common examples include Zeppelin NT, Norge, Italia and so on. Non-rigid airships or

blimps, a contemporary technology like semi-rigid airships, are gas-filled pressure vessels made of natural or synthetic fibre [2]. The hull (helium-filled vessel) is equipped with appendages like gondola, a set of propellers and a tail rotor [7].

Modern manned semi-rigid airships like CargoLifter and Zeppelin NT utilize carbon-composite frames that allow them to be light, huge and structurally sound [2]. These airships are earmarked for payload delivery with their advanced actuation to control pitch and altitude. However, smaller unmanned version of these airships achieve actuation with thrusters [11]. Most common configuration involves two thrusters for longitudinal propagation and one thruster for transverse movement [11]. Fig. 1.1 shows some of the modern unmanned airships with an airship hull that has its maxi-

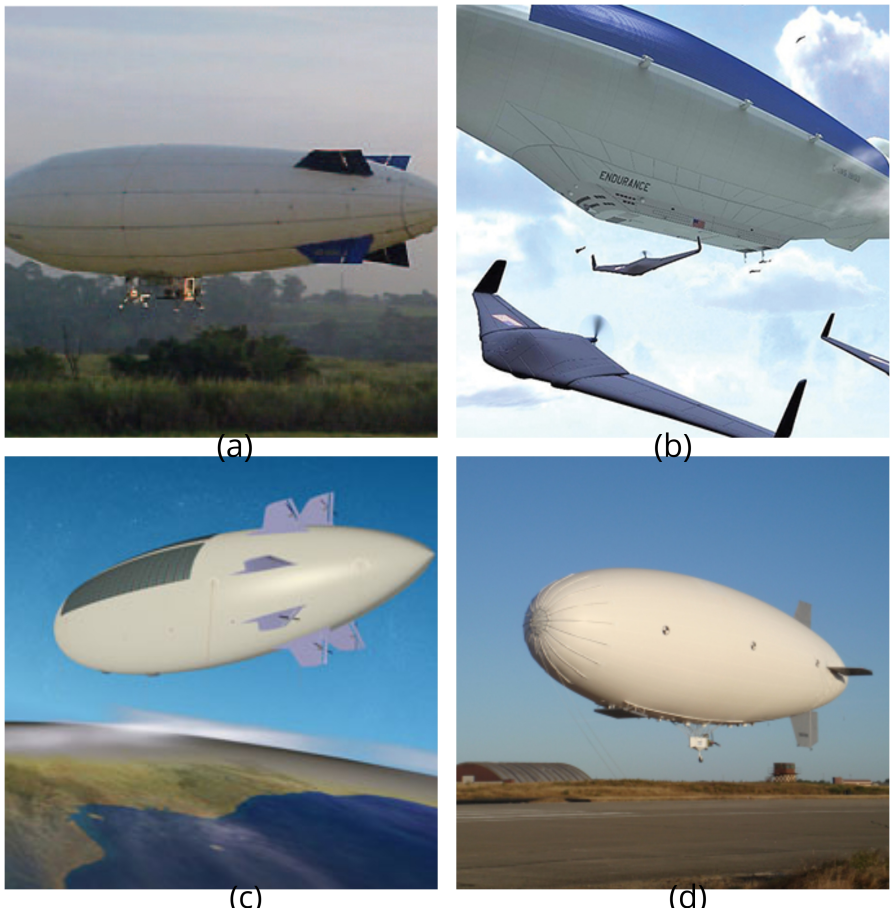

Figure 1.1: Modern unmanned airships: (a) Aurora airship AS 800 [8], (b) Airship deploying UAS [9], (c) High altitude airship Berkut [10], (d) SAIC Skybus 80K [9])

(a) Old airship model

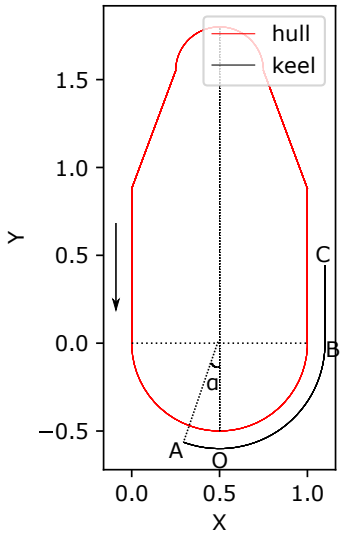

(b) Hull profile with keel for rapid descent

Figure 1.2: Structural modelling of semi-rigid airship: Old airship vs. new airship

mum diameter shifted away from the mid-section. These airships are either battery-powered or solar-powered or powered by combination of both. Despite this, the small unmanned airships are typically under-powered, under-actuated and lack controllability making them vulnerable to crash in adverse weather conditions [11][12][13].

To address the concern, the current research will attempt to use a center of gravity (CG) control for rapid descent capability as shown in Fig. 1.2. The descent is generally realized for neutrally buoyant airships as shown in Fig. 1.3 which shows the CG control using ballast repositioning instead of conventional over-actuation using controller [12]. A friction wheel is used to drive the gondola along the keel as shown in Fig. 1.4. It must be noted that no aerodynamic optimization was performed on the vehicle shown in Fig. 1.3 [11]. The present work proposes the fastest means to achieve descent by utilizing an extended keel (with a straight portion and a circular portion around the bow) embedded inside the envelope material as shown in Fig. 1.2(b). Design of an airship involves multiple complementing objectives that are often formulated into a single multi-objective optimization problems. Evolutionary algorithmic (EA) optimization techniques such as genetic algorithm (GA) are a robust

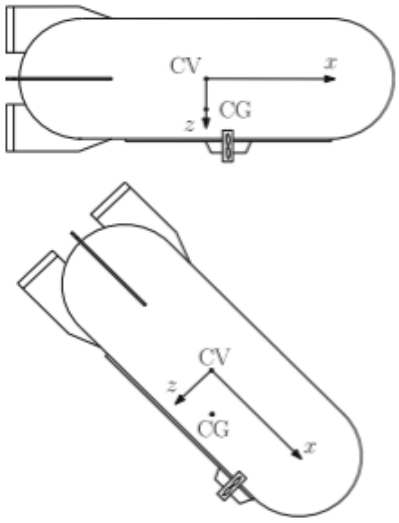

Figure 1.3: Airship descent using CG control [12]

and powerful technique to solve such optimization problems [14]. Consequently, a hybrid genetic algorithm (HGA), a combination of local search and global search techniques, is employed on the mathematical model of airship hull to optimize its surface area and aerodynamic drag for a given range of missions.

1.2 Problem description

The scope of the current research is restricted to the design optimization of the autonomous, semi-rigid airship described in the previous section. Earlier airships had a cylindrical shape as shown in Fig. 1.3 and ellipsoid form while modern airships have a prolate ellipsoid shape with lower fineness ratio [1]. The cylindrical hull facilitates a smooth sliding of gondola unit which has its significance while the ellipsoidal or prolate ellipsoid profile is proven to be aerodynamically superior [4].

To understand the dynamics, stability and control of the airship, the motion of axes is considered with respect to the trimmed equilibrium flight. For a general configuration of body axes, origin is assumed to be at the center of volume (CV), the x axis is coincident with the axis of symmetry and the oxz plane is coincident with the longitudinal plane of symmetry of the airship as shown in Fig 1.5. Considering that

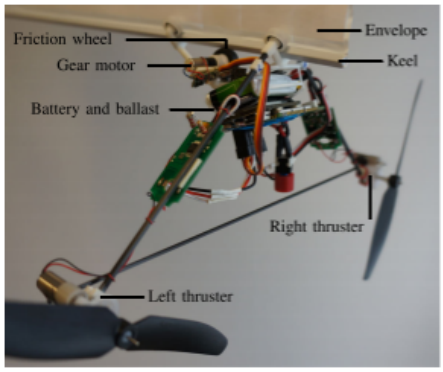

Figure 1.4: Airship gondola prototype [12]

the volume of gondola is negligible in comparison to the volume of the hull, the CV lies on the axis of symmetry of the envelope. A labeled, side view of gondola that also carries the ballast is shown in Fig. 1.4. The friction wheel, powered by a gear motor, is pressed against the keel to help the sliding movement of gondola. The two forward facing thrusters provide the necessary forward thrust.

In designing an airship, it is vital to consider the balance or trim of the airship. For any type of aircraft to be stable and controllable, it is necessary to have the CG to be within a prescribed range from the origin. In relation to airships, the relationship between the CG and center of volume (CV, geometrically located at the CB of the envelope) is of paramount significance. For instance, the CG should be vertically collinear with the CV for a statically stable configuration (ignoring the aerodynamic and thrust effects) [1]. Airship will adopt a pitch for any horizontal offset between the CV and the CG. Extending the concept to descent, the CG and the CV should follow the same relation to achieve the maximum pitch. Lanteigne *et al.* based on the study by Srikanth *et al.* suggested that a feasible way to achieve pitch control for a small unmanned airship is to exploit center of gravity (CG) control with the aid of a sliding ballast [11][13]. This is achieved by attaching a rail/keel to the bottom of the airship on which the ballast slides.

It is imperative to include the pertinent characteristics of an airship while consider-

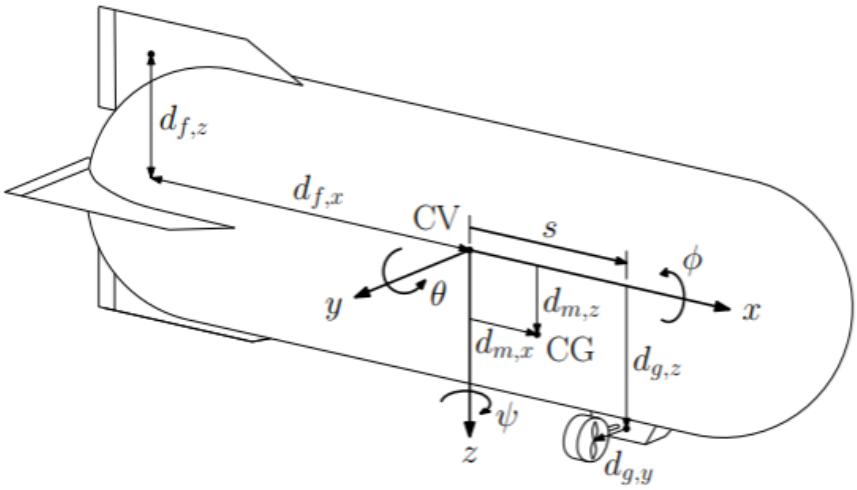

Figure 1.5: Airship axes configuration [11]

ing the conceptual design [15]. For instance, the structure of an airship including its weight, the aerodynamic effects on the vehicle, propulsive power needs (solar cells, if used) and so on are to be incorporated into the objective function. Envelope mass of an airship, which is a function of total surface area, has a significant contribution to the total self weight, and, thereby affects the payload capacity. On the other hand, the envelope body profile also influences the aerodynamic force and moments generated on it. To increase the payload capacity and reduce the required propulsive power of an airship, it is indispensable to optimize the envelope drag coefficient that accounts for roughly two-third of the total airship drag [16].

The objective is to optimize the shape of the airship hull for a given payload capacity subject to the effects of aerodynamics and the structural weight with the additional constraint of enabling a complete vertical pitch to improve controllability.

1.3 Thesis layout

The thesis will be comprised of six main chapters. A thorough review of existing literature on airship optimization will be summarized in Chapter 2. The methodology adopted for the current research will be presented in Chapter 3. Chapter 4 will highlight the simulation platform set up for optimization. In Chapter 5, the results obtained will be discussed and compared to relevant work by other scholars in addition to running the algorithm on commercial blimps. Finally, Chapter 6 will list the conclusion of the present research.

Chapter 2

Literature review

2.1 Airship shape optimization

In order to facilitate practical applications of unmanned airship technology, it is vital to enhance their operational efficiency. For instance, the propulsive power needed for an airship is a factor of the aerodynamic drag on the gas envelope. Optimizing the aerodynamic drag would enable higher endurance, low power consumption, less fuel (greater payload), and increase the range of missions. Propulsive power (P_{cr}) relates to the drag force at cruise in the following manner where, propulsive power,

$$P_{cr} = \frac{DV_{cr}}{\eta_{prop}} \tag{2.1}$$

where D is the drag force on the ship, V_{cr} is the cruise velocity, and η_{prop} is the propulsive efficiency [17].

It is significant to understand that airship optimization is not a novel idea. Early optimization attempts could be dated back to the last quarter of the twentieth century. Lutz *et al.* devised a tool for drag optimization of axi-symmetric airship bodies submerged in incompressible flow at zero incidence [16]. This work used a parametric source distribution function to model the body profile of the airship as shown in Fig. 2.1 and the source strength was modelled as the design variable. The prime objective of the work was to attain an aerodynamic shape for a prescribed range of flight speed (five Reynolds number regimes).

The authors employed a sophisticated semi-empirical e^n-transition method for predicting the location of transition of fluid flow from laminar to turbulent. The work was premised on the idea that the length of laminar flow region has a crucial impact on the drag coefficient, predominantly for lower to medium Reynolds number.

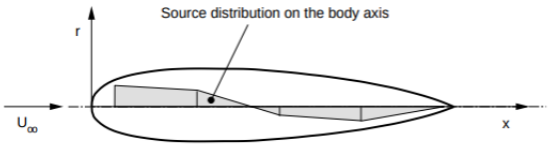

(a) Flow field at zero incidence

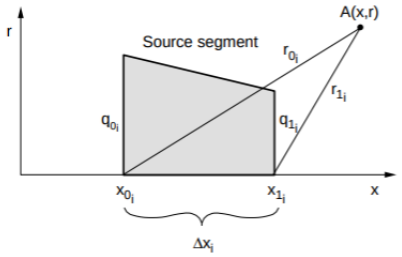

Figure 2. Source section with linearly varying strength

(b) Source section with varying linearly strength

Figure 2.1: Modelling of flow field and geometry of body profile [16]

They used POINTER, a commercially available optimization tool, and an evolution strategy with de-randomized co-variance matrix adoption tool to minimize the multi-dimensional objective function. In this work, no geometric constraint was introduced; instead the results were derived solely on the basis of friction and form drag with a penalty for pressure drag in case of turbulence. This method was computationally expensive and it ignored surface waviness of airships and the drag induced by attached bodies such as the gondola, fins, and thrusters.

A considerable number of attempts for multi-disciplinary design optimization (MDO) incorporating Structures, Aerodynamics and Flight Mechanics, can be found in the literature for improving airship design and performance [14] [18]. A classical strategy to incorporate the different domains is to formulate a pertinent objective function. This approach is commonly referred to as 'Sum of weighted function'. Nejati *et al.* extended the drag-based optimization of airship hull by using genetic algorithm (GA) [14]. Unlike other previous work, this work used a forced transition criterion

to identify the transition region with respect to Reynolds number. In other words, they replaced the transition region by a transition point i.e. 3% of the body length. Also, the boundary layer was calculated by neglecting the curvature effects which led to error in results at the stern side of the ship. The drag coefficient was computed using Young's expression as shown below:

$$C_D = \frac{4\pi r_0 \theta}{S}(U_e^*)^A \tag{2.2}$$

where,

$$A = \frac{H+5}{2},\ S = \pi[(r_0)_{max}]^2 \tag{2.3}$$

where C_D is the drag coefficient consisting of form drag and skin-friction drag, θ is the momentum thickness, A is the area factor, H is the shape factor, U_e^* is the velocity at the edge of the boundary layer, S is the surface area at maximum radius, and r_0 is the radius of the body of revolution.

Pant established a methodology for determining baseline specifications for non-rigid airships [17]. The research provides a benchmark for conceptual design of an airship with a platform for multi-disciplinary optimization for a certain payload capacity. Mueller *et al.* emphasized the importance of a superior control and guidance system for an unmanned autonomous airship [19]. They developed a dynamic model of the airship based on energy balance and mass constraints, and they achieved an aerodynamic model of the double-ellipsoid airship profile using computational fluid dynamics (CFD) tools [19]. This work stands out in designing control laws for single operating condition based on results from open loop dynamic tests translating to a representative model for expected disturbances. Put another way, linearized models of the open-loop dynamics were used to build SISO controller for tracking desired angular and linear velocity. Thus, Mueller *et. al*'s investigation involved the shape optimization of the hull together with the design of control laws corresponding to the airship. Kale *et al.* argue that the drag coefficient estimation on the basis of empirical relation by Hoerner and Cheeseman concurs to the results from CFD packages for only a specific class of envelope shapes [20]. This class is based on values of fineness

ratio and the position of maximum diameter along the longitudinal length of the airship. The empirical relation is as follows [1]:

$$C_{DV} = \frac{0.172(l/d)^{1/3} + 0.252(d/l)^{1.2} + 1.032(d/l)^{2.7}}{Re^{1/6}} \tag{2.4}$$

where the Reynolds number is expressed as

$$Re = \frac{\rho_a v d}{\mu} \tag{2.5}$$

where C_{DV} is the volumetric drag coefficient, l and d are the length and the maximum diameter of the airship respectively. Re is the Reynold's number, ρ_a is the density of air, μ is the dynamic viscosity of air, and v is the velocity of wind.

Consequently, they devised a response surface methodology (RSM) based on geometric parameters to ascertain the relation between parameters involved and the drag coefficient. The RSM technique further optimized the objective function over the design space and a second-order surface fit was obtained to predict the drag coefficient values with an accuracy of $\pm 10\%$. Wang *et al.* presented a methodology for multi-objective optimization of airships based on aerodynamics, structural stresses primarily, hoop stress, propulsive power and, the area of solar array [21]. They suggest that a user can choose from multiple optimizing algorithms, namely ASA, NSGA-II or NLPQL to achieve an optimum shape that is modelled on the basis of shape generation algorithm. The shape is modeled on the basis of airship equation as shown:

$$64(y^2 + z^2) = a(l - x)(bx - l\sqrt{c} + \sqrt{cl^2 - dlx}) \tag{2.6}$$

such that a, b, c and d are the independent variables used to represent the shape coefficients of the airship shown in Fig. 2.2.

The body profile generated using the equation and the constraints can be seen in Fig 2.2. Gawale *et al.* presented a detailed methodology for remotely controlled (RC) airship design, sizing and layout based on user-specified performance and operational needs [4]. They showed that stability and control requirement also suit the

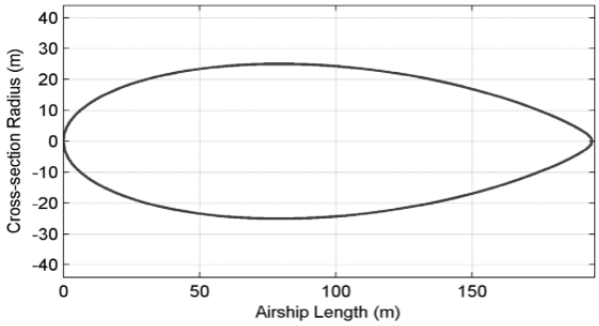

Figure 2.2: Modelling of geometry of body profile

slender shape of the airship. The study also offered a detailed discussion on the standard envelopes, material to be used for envelope, fin sizing, lift calculations, and the propulsion system. They proposed that the envelope fabric thickness was a function of circumferential and longitudinal stresses acting expressed as follows:

$$\sigma_{hoop} = \frac{\delta P_{int} 2r}{2t} = \frac{\delta P_{int} r}{t} \tag{2.7}$$

$$\sigma_{long} = \pm \frac{BMr}{\pi r^3 t} \tag{2.8}$$

where σ_{hoop} and σ_{long} are circumferential/hoop stresses and longitudinal stresses per unit width respectively. Also, δP_{int} is the internal pressure of the hull, and r and t are the radius and thickness of the fabric respectively. BM is the bending moment on the envelope.

Wang *et al.* performed MDO including factors such as weight, aerodynamics, structure and energy using adaptive simulated annealing (SA) [15]. Along these lines, Ram *et al.* presented a comprehensive optimization of the aerostat envelope including fin sizing for static stability of the tethered body [22]. They showed the importance of multi-fabric construction that can improve the payload capacity by around 6.5%. The focus of their research was to achieve an airship that can be static for wide range of atmospheric disturbances. Furthermore, they showed calculations for weight of the fin for a stable configuration and the forces on each tether element shown in Fig. 2.3 with respect to the confluence point. For this type of airships, blow-by is a major

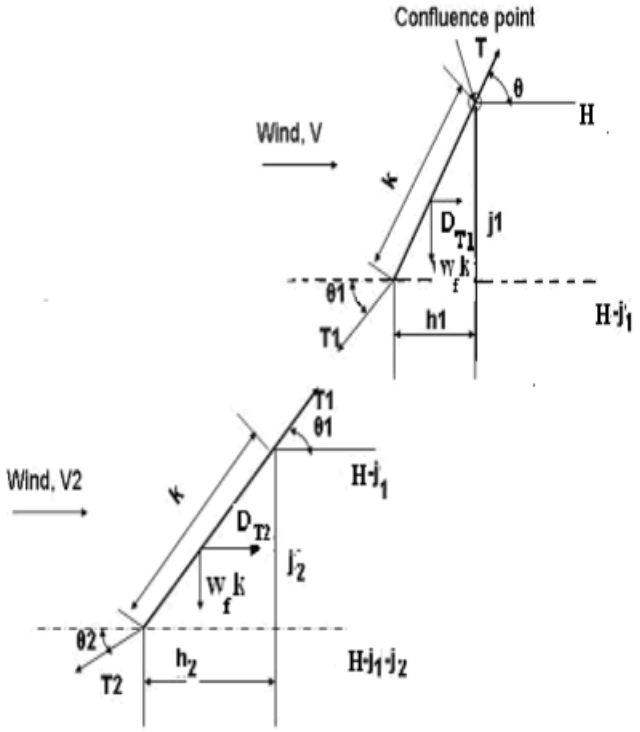

Figure 2.3: Forces on tether elements with respect to confluence point [22]

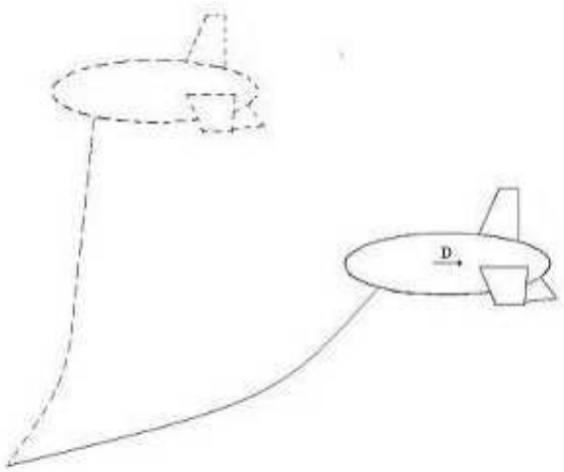

Figure 2.4: Change in operational height due to blow-by [22]

cause for concern [22]. Blow-by refers to longitudinal displacement of the aerostat due to wind drag. Thus, to retain a constant operational altitude, a longer tether is needed as seen in Fig. 2.4. Also, the longer the tether, greater is the weight. Thus, a lot of effort is put into optimizing the tether profile [22][20]. Concurrent subspace optimization based on response surface approximations is performed in the literature for conceptual design of high altitude airships [23]. Liang *et al.* attempted to optimize the envelope shape and location of solar array for minimum total mass [23]. Other evolutionary algorithmic optimization techniques like particle swarm optimization (PSO) and simulated annealing (SA) are also employed for the MDO of airships as reported in the literature [24]. Optimization of airships with certain unconventional contributions is presented by Amani *et al.* [18]. In their research, the glide distance traveled by the vehicle in a given time is adopted as one of the objectives based on the argument that a larger helium mass is required for a larger distance. In order to achieve the static stability, stability derivatives are optimized subjected to initial disturbances.

To put GA in the context of modern developments in the field of artificial intelligence techniques of optimization, the next section is included to give the reader a basic understanding of optimization strategies. The terminology used in the evolutionary techniques is very uncommon in the core of mechanical engineering and thus, a brief genetic background is supplied to further the understanding of terms and rationale behind the components of the algorithm.

2.2 Optimization methods

Engineering optimization can be defined, mathematically, as a process of finding conditions to minimize a function provided that the constraints, if any, do not fix the solution in the feasible domain [25]. The general process of optimizing an engineering problem can be summarized as shown in the flowchart shown in Fig. 2.5

The need for optimization should be identified firstly such that it does not preclude

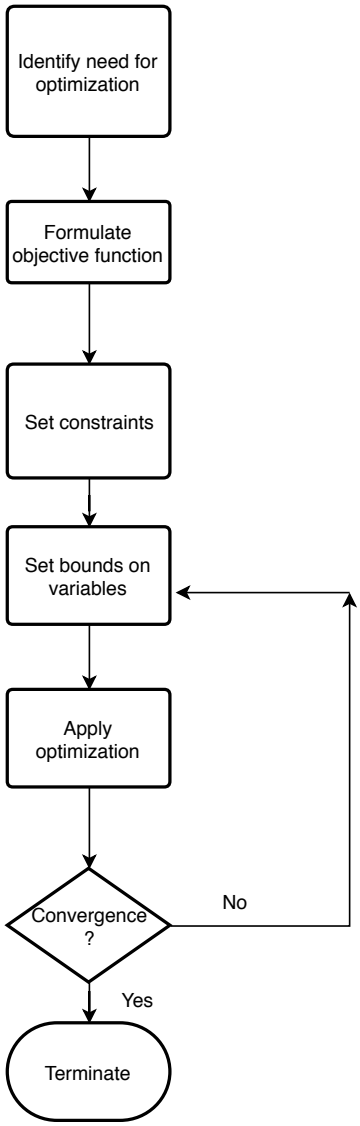

Figure 2.5: Optimization flowchart [26]

any of the methods of optimization [25][26]. Subsequently, it is necessary to formulate the engineering problem into a mathematical model, that is, optimized for a set of constraints with a bounded set of variables until the convergence criterion is met. Quite notably, it is a common engineering practice to limit the design space based on the practicality of a design [26].

Optimization techniques can be broadly classified on the basis of the nature of the

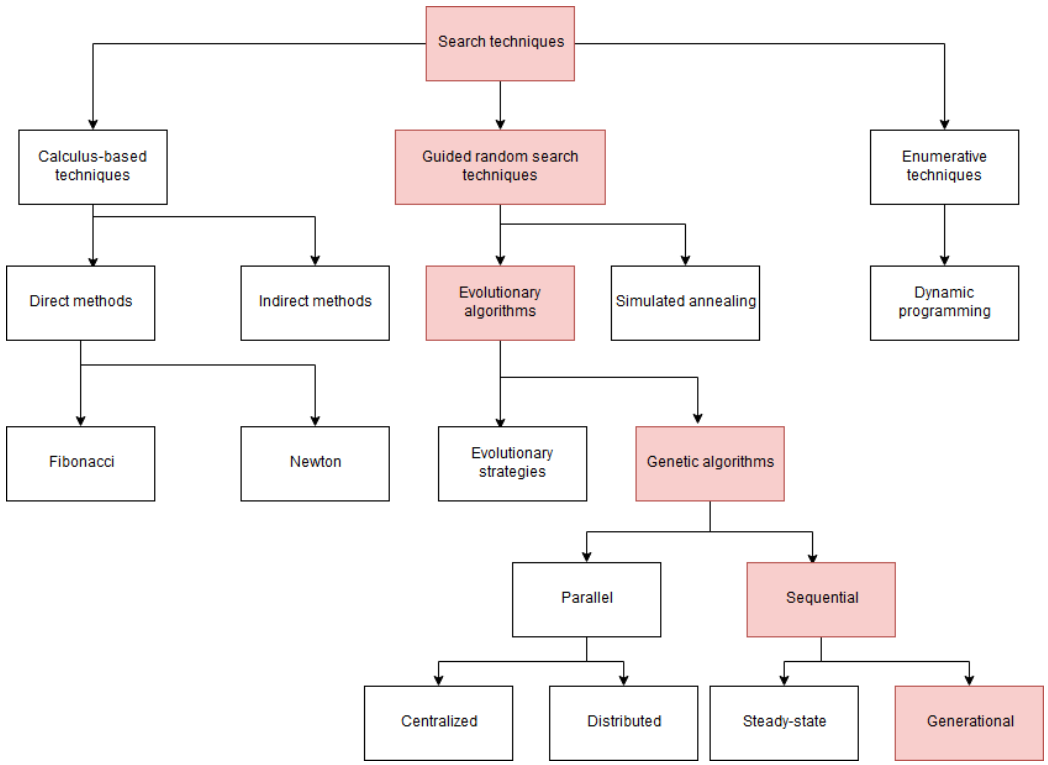

Figure 2.6: Optimization methods [25]

problem and the method of solving as shown in Fig. 2.6. Optimization methods can be broadly categorized into calculus-based techniques, guided search strategies and enumerative techniques. In traditional optimization techniques such as calculus-based methods that is classified into direct and indirect methods, the convergence to an optimal solution relies on the chosen initial solution that is used for the first iteration [27]. Moreover, these methods tend to be inefficient for discrete variable problems and they cannot be used on a parallel machine. Direct methods utilize the knowledge of objective functions and constraints to steer the search for optimum [27]. On the other hand, indirect methods or gradient-based methods use first and/or second-order derivatives to find the conditions for optimum [27]. Owing to this, they are inefficient for discontinuous or non-differentiable problems. For a non-linear and complex problem, the traditional techniques are only sophisticated enough to solve for local optimum, hence, they are not suitable for multi-modal problems. The most powerful calculus-based indirect method, the Lagrange multiplier method, states that for a constrained problem, the optimum is reached when the following condition is

satisfied:

$$\delta y - \lambda \delta \phi = 0 \qquad [28] \tag{2.9}$$

where λ's are the Lagrange multipliers, y is the objective function matrix and ϕ is the constraints matrix. It is to be noted that each traditional technique is tailor-made for a specific type of problem [27]. For instance, for a convex problem with differentiable design space, the optimization process is much faster with indirect techniques as compared to any other method as described in section A of Appendix. Some of the most eminent calculus-based direct methods include- the Fibonacci and Newton methods.

Enumerative techniques, such as dynamic programming in which the entire problem is divided into a sequence of elemental problems, demand considerable creativity in the optimization process. The applicability of these methods is also limited to the type of problem [25]. For instance, geometric programming is designed to optimize polynomial-type cost functions and constraints, the conjugate gradient methods are known to converge for quadratic cost functions and so on. Obviously, Fig. 2.6 does not show an exhaustive list of all known optimization techniques. Other similar methods include linear programming, geometric programming, etc [25].

The third major class of optimization methods is search methods. Search methods like evolutionary techniques tend to mimic natural evolution in the form of a progressive improvement in the solution throughout the search for optimum. These methods do not have any mandatory requirement for continuity or differentiability of the objective function [28]. Some of the popular evolutionary algorithms (EAs) are particle swarm optimization (PSO), simulated annealing (SA), ant-colony optimization (ACO), differential evolution algorithm (DEA), tabu search etc. PSO is a stochastic search technique inspired from the social behavior of bird flocking or fish schooling [28]. In PSO, each feasible candidate solution is adjusted through the search space following the behavior of their neighboring candidates. Like PSO, simulated annealing (SA) is also a robust meta-heuristic method to solve for a larger search space [21]. Inspired

from the minimum energy configuration of metals during annealing, SA tries to minimize the objective function where cost is analogous to the energy of a state of metal. On the other hand, Genetic Algorithm (GA) is a stochastic search algorithm based on the mechanics of genetics and natural selection [29]. Based on the premise that natural evolution is an optimization process, GA simulates the process of evolution. GA is proven to be a robust and powerful technique that features a remarkable balance between efficiency and efficacy. In engineering terms, it explores and exploits the feasible design space at a promising rate, that is to say, finds the global optimum.

Quite evidently, GA has been a preferred optimization technique in airship design and optimization in the pool of evolutionary artificial intelligence algorithms [14][22][18][30]. Nejati *et. al* used GA for the first time to estimate aerodynamic calculations for the airship bodies without any tail fins [14]. Ram *et. al* proposed an optimized shape of aerostat envelopes using GA to ascertain the optimum shape for single and multi-fabric configurations [22]. Amani *et. al* presented an optimized airship model for the following objectives- drag, stability and traveled distance. In addition, the optimal design on the Pareto front was also estimated [18]. Along the same lines, a multi-disciplinary shape optimization of stratospheric shapes using GA incorporating solar cell area as one of the objectives is presented by Alam *et. al* [30]. Appreciating the importance of GA as a robust global optimization scheme, the current work employs GA to optimize the shape of unmanned, semi-rigid airship.

2.3 GA in detail

Genetic algorithm has four main components: encoding, selection, crossover, and mutation. GA starts by creating a population pool of random feasible individuals that, in turn, undergoes a selection filter based on fitness. The selected individuals participate in crossover to produce new off-springs that replace the individuals that were not selected. Some of the individuals, subsequently, undergo mutation in order to bring in new genetic content (explore the search space) [31].

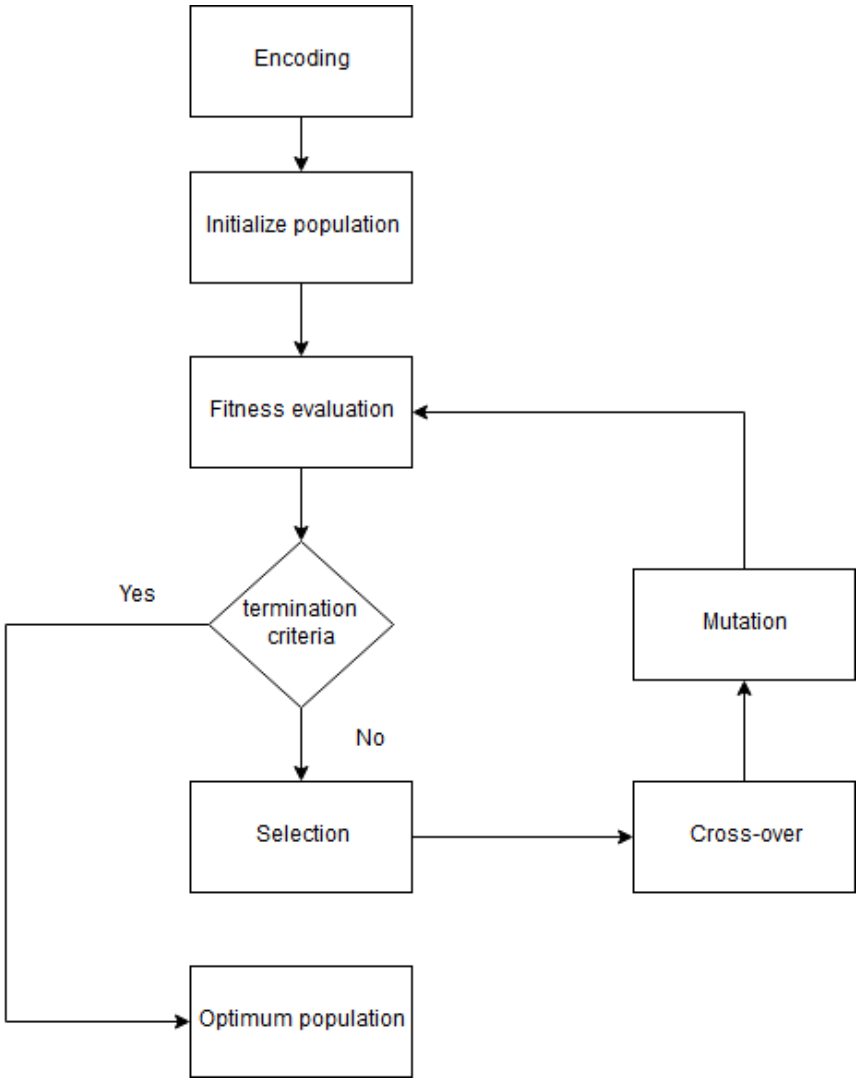

Figure 2.7: GA operators

The flowchart shown in the Fig. 2.7 gives a general overview of the GA operators in sequence. A more detailed description into the algorithm operators and the nuances of the various options is as follows:

Encoding: The individual representation in the algorithm is referred to as encoding. There are two important ways to encode each chromosome: binary representation and floating-point representation. Floating-point or real-valued GA is an order of magnitude superior in terms of computer CPU time as compared to binary GAs [29].

$$\text{chromosome} = [10101 \quad 01010 \quad 10101 \quad 01010] \tag{2.10}$$

$$\text{chromosome} = [p_1 \quad p_2 \quad p_3 \quad ...p_n] \tag{2.11}$$

The above equation 2.10 shows the binary representation for a chromosome with four variables while equation 2.11 shows the representation for floating point or continuous GA. Understandably, the size of an individual will be much larger to represent a floating point number in binary which will, in turn, affect the total storage requirement. Floating point GA does not have to be decoded at the end of the algorithm making them inherently faster than binary GA. It is also suggested that more natural representation produces better solutions [32]. In general, many researchers have concluded that GA is superior to other optimization algorithms for a wide range of problems [14][30][22][18][2][32].

Fitness evaluation: The encoded individuals in the population are arranged in the order of increasing fitness function values. The fitness/objective function value of each individual is evaluated as per the objective function described in section 4.1, such that the first chromosome in the vector is the optimum design candidate and has the lowest value of objective function value for a minimizing objective.

Selection: Pairing or selection in GA can be achieved in myriads of ways. Some of the interesting methods are [29]:

• Top to bottom pairing: In this, the chromosomes from top to bottom are paired two at a time until N_{keep} i.e. the number of individuals deemed fit enough to pass onto the next generation is reached.

• Random pairing: As the name suggests, parents are randomly selected by using a random number generator that is further used to call on different rows.

$$mg = np.ceil(N_{keep} * random.rand(N_{keep})) \tag{2.12}$$

where mg is the row vector that stores the row numbers to be selected for pairing of chromosomes and N_{keep} is the number of chromosomes passed on to the next generation.

• Weighted random pairing: As the relative importance of an individual in a pool

is dependent on its cost, probability of selection is assigned to each individual such that one with the least cost has highest chances of getting picked and vice-versa. The individuals are subsequently selected as the cumulative probability of the pool is greater than the generated random number. This method is also known as roulette wheel selection [29].

$$P_n = \frac{N_{keep} - n + 1}{\sum_{n=1}^{N_{keep}} n} \tag{2.13}$$

where P_n is the probability of selection of a chromosome in the pool based on its fitness, n is the rank of the chromosomes in the pool.

• Tournament selection- This method of selection also quite closely mimics the natural selection. In this, a small subset is randomly selected out of the population, and the best individual from that pool is chosen to be the parent. This process is repeated until all the parents are selected [29]. Tournament selection is a magnificent technique for large populations as other methods tend to get slower with increasing population size.

Crossover: Crossover or mating is a process of creating new individuals by maintaining the genetic makeup of the population. A very common approach of crossover is the one in which two parents produce two off-springs. The point of crossover (kinetochore) is randomly chosen out of all the genes of a parent for single point crossover. Consequently, the genes are exchanged between the parents. Let's suppose, the crossover points come out to be genes (2, 3, 6). Therefore, only those genes are exchanged in the crossover process as shown in the illustration below.

$$mg = [p_{m1}\ \ p_{m2}\ \ p_{m3}\ \ p_{m4}\ \ p_{m5}\ \ p_{m6}\cdots\ \ p_{mn}] \tag{2.14}$$

$$fg = [p_{f1}\ \ p_{f2}\ \ p_{f3}\ \ p_{f4}\ \ p_{f5}\ \ p_{f6}\cdots\ \ p_{fn}] \tag{2.15}$$

$$c_1 = [p_{m1}\ \ p_{f2}\ \ p_{f3}\ \ p_{m4}\ \ p_{m5}\ \ p_{f6}\cdots\ \ p_{mn}] \tag{2.16}$$

$$c_2 = [p_{f1}\ \ p_{m2}\ \ p_{m3}\ \ p_{f4}\ \ p_{f5}\ \ p_{m6}\cdots\ \ p_{fn}] \tag{2.17}$$

where mg and fg are the mother and father chromosomes respectively, producing the child individuals c_1 and c_2.

While for a uniform crossover, it is randomly decided which parent will contribute to a position of an offspring for certain number of pre-decided crossover points [29]. The main problem with this approach of mating is that no new information is brought into the genetic pool. Put another way, the same floating-point numbers are exchanged and propagated throughout the generations. So, the onus to introduce new material (explore search space) shifts entirely to mutation. To solve this setback, blending method of mating is adopted [29]. In this, the new off-springs variables are a combination of two corresponding values in a random proportion [31].

$$OS_x = \beta p_{mx} + (1 - \beta) p_{fx} \tag{2.18}$$

where β is a random number generated, also called the mixing parameter, on the interval [0,1] and OS_x is the blended gene using the parents genes p_{mx} and p_{fx}.

Mutation: Mutation in a GA refers to the process of alteration of one or more genes in a chromosome to address genetic diversity in a biological population. It is customary to include mutation in the entire evolution-"mimicking" to avoid premature convergence of the algorithm [31]. Mutation aids to ensure that the search space is satisfactorily explored by adding in new information (genetic material). The most common way to achieve this is to replace the mutated variables by a new random variable that is within the bounds of variables. This approach is commonly referred to as random mutation.

Hybrid GA: It is very well established that regular GAs are not suited to fine tuning and modifications to tackle complex search spaces [33]. Furthermore, recent advancements in the implementation of genetic algorithm have proven to be advantageous by greatly improving the efficiency. Evidently, it has been noticed in the literature that GA gravitates speedily to a global minimum. However, it is not sophisticated enough to close-in on the global optimum when in a locally quadratic region [29]. It is common to hybridize simple GA with local search technique, thereby, making it a hybrid genetic algorithm (HGA) or memetic algorithm (MAs) [34]. That being said,

it is extremely critical to decide a necessary balance of the exploration action of local optimization over the exploitation action of the GA [35]. There are several ways to employ HGA [29]:

- Run GA until the performance slows down, then allow the local optimizer to take over. It is assumed that the solution passed on is already in the neighborhood of the global minimum.

- GA is seeded with a population that has evolved at some random point in the population at any random gene. Now, the most common approach to achieve this is to use hill climbing (HC) technique after the mutation stage. Hill climbing is a common local search method that usually starts with a single solution point. Subsequently, at each iteration, a feasible solution is generated with the help of a move operator. This move operator could either be a crossover (shown in the psuedocode 1) or a random number generation. In a nutshell, the algorithm builds up on the optimization from an arbitrary solution, that is progressively improved by making incremental changes to the solution. There are several implementations of hill climbing proposed in the literature- crossover HC, random HC. Unlike crossover HC, in random HC the offsprings are created randomly within the bounds of variables [34].

- After a number of generations, run a local optimizer on the elite class (optimum candidates and/or their neighboring candidates for each iteration) and modify the population accordingly.

Algorithm 1 Pseudocode- Crossover hill climbing (p_1, p_2, n_0, n_i)

1. $p_1' = p_1$ and $p_2' = p_2$
2. For n_i generations:
3. Generate n_0 offsprings by mating p_1' and p_2'
4. Calculate the fitness of new offsprings.
5. Find best offspring
6. Replace the worst of p_1' and p_2' with best offspring.
7. Return p_1' and p_2'

2.4 Pareto optimality

Even though it is very tempting to solve a single objective problem, most of the real life problems are multi-objective, and to aggravate the situation, the knowledge of search space is relatively limited for the latter as compared to that for the former. Furthermore, in an MOOP, since there are several objectives conflicting with each other, there is no single optimum solution for various weights for the objectives of the problem. Instead, a set of equally good solutions for the range of weights exists, and is sought. Consequently, there could be best solution, worst solution, and solution indifferent to other solutions (non-dominating, non-dominated) [36]. However, the

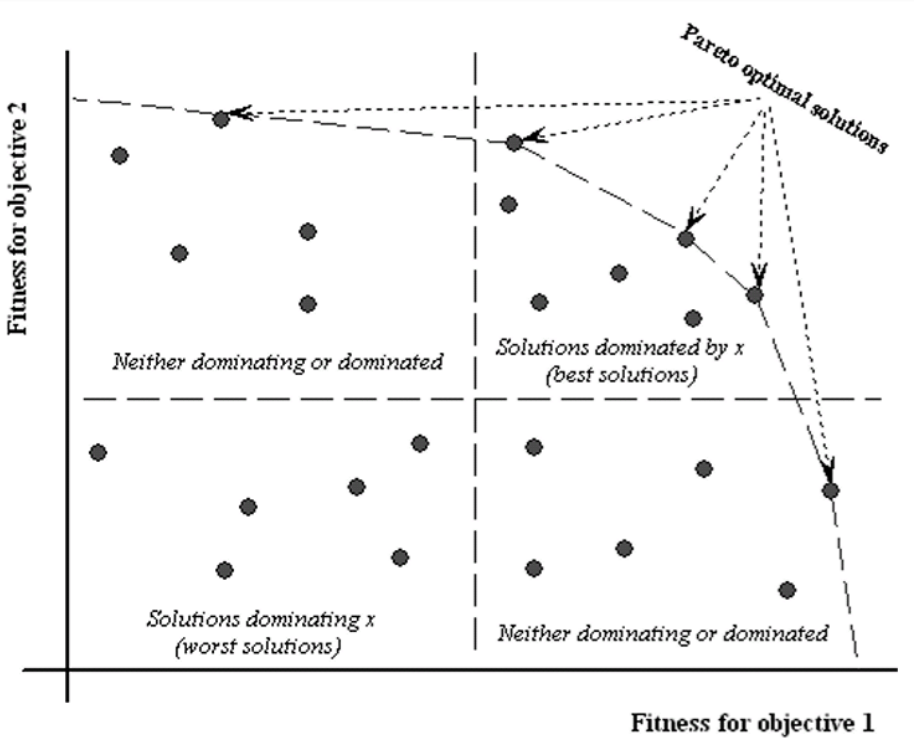

Figure 2.8: Pareto optimality [36]

optimal solution is the one that is not dominated by any other solution in the search space as can be seen in Fig. 2.8. The figure shows the best solutions in the quadrant 1, worst solutions in the quadrant 3, and the non-dominating, non-dominated solutions in the quadrants 2 and 4 on a plot for two distinct objective functions that are a function of an independent variable vector $\mathbf{x}$. The optimal points shown in the figure

were defined as Pareto-optimal points after Vilfredo Pareto, an Italian engineer and economist [37]. These points lie on the Pareto front represented by the curve. The Pareto optimal solutions are always of prime interest in a multi-disciplinary optimization (MDO) owing to the fact that they suggest a group of optimal solutions for a variation in the importance of an objective with respect to the other. In practice, in order to make sure that a better approximation of Pareto front is obtained, a larger population set is needed in comparison to the MOOP method of 'sum of weighted objectives'.

There has been a significant growth in the approach to solve multi-objective problems using multi-objective evolutionary algorithm (MOEA) [38]. For such problems, the decision maker needs an approximation to the Pareto-front to make a preferred decision in the design process usually accomplished by evolutionary algorithms. Prior to selecting a suitable technique for this, it is vital to visualize the search space in design space and criterion space.

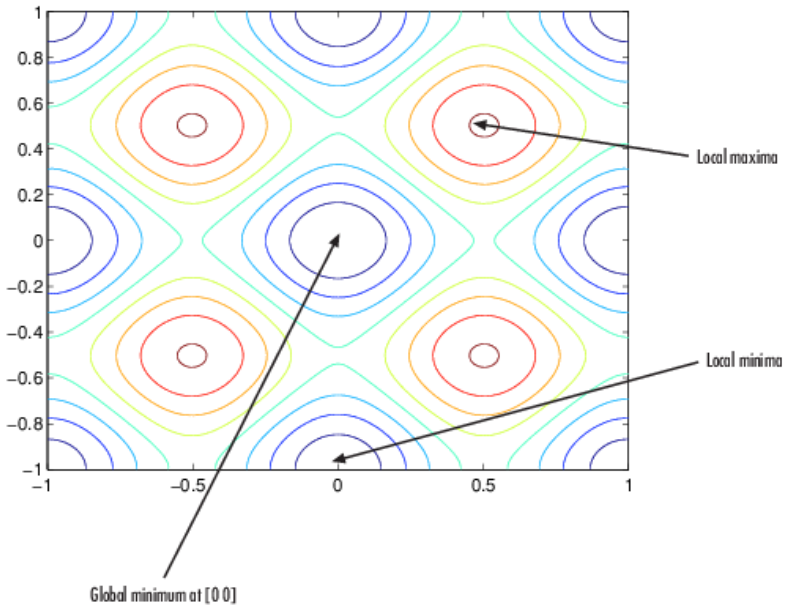

Figure 2.9: Design space [39]

An objective function along with the constraints could be depicted in design space

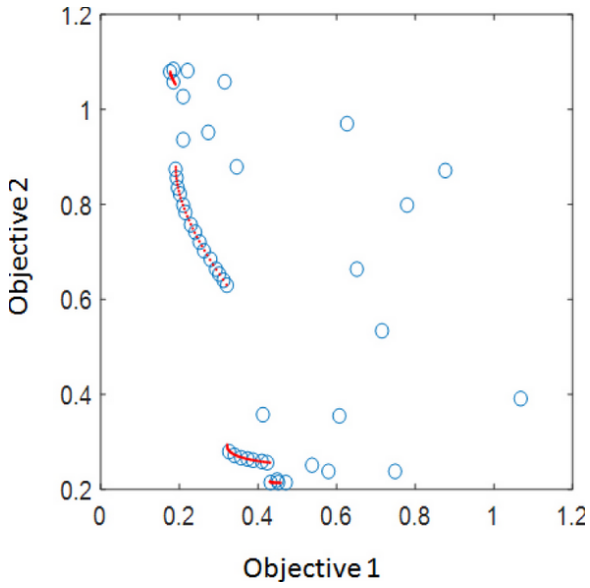

Figure 2.10: Criterion space [39]

in which the functions are plotted with the design variables as the axes as shown for illustration purpose in Fig. 2.9.

On the contrary, the multi-objective optimization function could also be depicted in criterion or cost space as shown for illustration purpose in Fig. 2.10. In this, the axes are represented by the value of different objective functions. The red lines formed by the cluster of points represent the Pareto optimal points for a minimizing objective function problem. As can be seen, the points on the curve are dominating all the other solutions for the same value of objective functions (i.e. all other solutions horizontally and vertically).

The Pareto optimal set is always situated at the boundary of the feasible criterion space [28]. Despite that, the Pareto front is not necessarily defined by the constraints. In fact, the Pareto front exists even for unconstrained multi-objective problems.

Chapter 3

Modelling and theory

This chapter illustrates the modelling of the low-altitude airship, the methodology adopted for the optimization process and the overall optimization approach employed for the current research. A mathematical model of the ship will be proposed to parameterize the shape in order to express all the structural features vis-à-vis structural strength, aerodynamics, equilibrium control, size effects and, shear forces and bending moment considerations acting on the airship hull structure.

3.1 Modelling of the airship

Referred to as 'unmanned aircraft systems' (UAS) by various western regulatory organizations, even so not distinct from 'remotely piloted vehicles' (RPV), unmanned airships are bound by the same concepts of aerodynamics, weight, performance and aerostatics as manned airships [1]. The term UAS encompasses a piston or jet-driven or any electric motor propulsion systems. The present work is meant to address the design concerns of a radio controlled (RC) airship as well as that of an autonomous airship. Besides, RC airships configuration due to their low weight and absence of a well-equipped launching needs, are free of any certification requirements in most countries with a little to no restrictions [40][1]. Unlike autonomous airships that are enabled to 'think' and take decisions independently i.e. without any human involvement, RC airships have manual and automatic mode for the flight control of the vehicle [1]. These unmanned airships could be as small as 0.06 m^3 in volume. Because of the nascent stage of the industry, the clear set of objectives ranked in priority are a driving force in the conceptual design of the airships.

Canadian Aviation Regulations (CARs) in Transport Canada define airships as- engine driven, lighter-than-air aircrafts that can be steered [41]. Airship standards are

laid commonly in the 'Airworthiness Manual Chapter 541' for both small and large airships. Regulations state clearly that hydrogen cannot be used as the lifting gas. They also require an extremely maneuverable unmanned air vehicle (UAV) to have a safety flight operation certificate (SFOC), and this necessity is also extended for tethered UAVs. Detailed regulations regarding standards for airships are reported under the same category as UAVs [42]. Transport airship requirements (TARs) states certain important guidelines for near-equilibrium non-rigid airships for both horizontal and vertical take-off and landing [43]. The document is a comprehensive compliance standard that should be followed in the design and manufacture of airship. TAR 21 Proof of compliance states that certification is issued for each appropriate combination of static heaviness, lightness, total mass, center of gravity [43]. The guidelines explain the allowed tolerance on the flight testing parameters. The maximum mass of the airship must be established before compliance is issued. Removable ballast is also permitted to be shown in compliance provided it is properly carried and installed on the airship. The maximum pitch is to be within a limited range so that the compliance is shown. The circumstances for take-off, landing and climbing are to be clearly stated to show compliance.

The key design drivers for the present airship conceptual design are as follows:

3.1.1 Weight

The total weight of the airship is determined by the payload, the envelope mass, the gondola, and the fuel carried by it. It is established that unmanned airships can fly upto 30% heavier than the displaced weight as opposed to manned airships that are limited to about 10% due to human accommodation requirements [1] [2]. The implication of flying with static heaviness is an aggravated aerodynamic drag and the related increased fuel needs [1]. Due to which, the airship will have to fly all the time in order to evade possible unwanted landing.

Static heaviness, quantified in kilograms or pounds, is the measure of the weight off-

set from the state of static equilibrium or neutral buoyancy of a ship [2]. In other words, it is the case when an airship has a higher weight than the displaced weight of the air, hence called heavier-than-air (HTA) airship. On the other side of the scale, are the airships with the maximum magnitude of static lightness. Thus, it is not hard to guess that there is an operational bracket for airships between extreme lightness and extreme heaviness [1]. That being said, it is customary to operate an airship slightly heavier (statically heavy) to facilitate easier landing. The importance of static heaviness is vital in case of emergency situations, adverse weather conditions and maneuvering. At the time of take-off or landing, the engine is kept idle and the ascend or descend rate is proportional to the static heaviness of the airship. Not to mention, the maximum efficiency is always at the static equilibrium of the airship because a relatively lesser power is required to maintain a certain airspeed. Static heaviness is commonly achieved by one of the following ways:

- An additional weight, also called ballast, used in the heaviness limit of the vehicle.
- Jettisonable payload in the form of fuel etc., a resort for hostile weather conditions.
- With relative lack of control, weather effects such as moisture on the hull or super-heating of the inflated gas.

Keeping in view the miniature size of the airship at cruising speed and its efficiency, a neutrally buoyant airship is designed for the present research. Owing to which, it will ride lighter and statically neutral and will achieve descent with the aid of the sliding gondola.

3.1.2 Altitude

In the conceptual design formulation, it is indispensable to consider the operational altitude above the sea level. For one reason, the increase in altitude has a dramatic impact on the volume of the airship needed to sustain the flight [19]. For instance, to lift 1 tonne of payload at sea level, the volume of the airship should be 816 m^3. However, a volume of 1105 m^3 is needed for the same mass of payload at 10,000 ft

above the sea level. On a side note, a typical operational altitude for small airship is 1,000 ft [1].

Based on the flight parameters like the weight of the gondola, the ballast weight, the wind speed, the temperature of the flight space, and the height of the flight, the flight data is seeded to the algorithm to compute the density of air and helium. For this work, we have assumed a 70 m altitude above the sea level that is the average elevation of Ottawa, a temperature of 15^o C as mean sea level (SL) conditions, and proceeded with calculations accordingly. The flight is limited to the lower region of the atmosphere i.e. troposphere. The temperature at the height is computed as follows[1]:

$$T = T_0 - Lh \tag{3.1}$$

where T is the temperature at a height h, T_0 is the temperature of atmosphere at sea level, and the pressure is given by:

$$P = P_0\left(1 - \frac{Lh}{T_0}\right)^{\frac{gM}{RL}} \tag{3.2}$$

where P is the pressure at elevation h, L is the temperature lapse rate, g is the gravitational acceleration, M is the molar mass, and R is the ideal gas constant= 8.314 $J/mol\,K$. thus, using the above equations, the density of the fluids is calculated using the ideal gas equation as follows:

$$\rho = \frac{PM}{RT} \tag{3.3}$$

3.1.3 Speed

Speed of travel for an airship is also a paramount issue in the conceptual design stage. The empirical relation between the power requirement and the speed of an airship can be approximated by:

$$P_i \propto S^3 \text{ [44]} \tag{3.4}$$

where P_i is the power needed to achieve a flight speed S. Thus, it can be said that there is a rapid escalation in the power requirement after a certain breakeven point.

Typically, for small airships, this point is around 80 knots (148.16 km/hr) [1]. For the current research, the angle of attack is considered to be zero and the travel speed is taken as 3.61 m/s or 13 km/hr for the aerodynamic drag calculation purposes, that is also the mean wind velocity used in the relevant literature for trajectory planning of airships [45]. Needless to mention, the input values of the atmospheric parameters are chosen only for the proof of concept and hence, could be altered to reflect the exact conditions.

3.1.4 Aerodynamics

A significant amount of aerodynamic literature suggests there are several ways to ascertain the aerodynamic drag on the airship. Wind tunnel testing for a scaled airship model for upto three different scales could be plotted to suggest a trend in the magnitude of lift and drag coefficients [1]. Usually, CFD analysis of the model is used to establish the credibility of the experimental results for the scaled model [46]. Furthermore, the drag coefficient for an airship could also be estimated analytically using empirical relations. Kanikdale *et al.* developed an empirical procedure based on experimental results from CFD analysis of numerous shapes for computation of C_{DV} as follows [47]:

$$C_{DV} = A\alpha + B \tag{3.5}$$

where the coefficients A and B are functions of the thickness ratio (d/l) [47];

$$\alpha = \alpha_1.\alpha_2^{\beta}.\alpha_3.X_{ymax} \tag{3.6}$$

and

$$\beta = \begin{cases} \frac{214}{(l/d)} - 31.26 & \text{for } \beta > 3 \\ 3 & \text{otherwise} \end{cases} \tag{3.7}$$

where parameters of α_1, α_2, and α_3 are as follows:

$$\alpha_1 = \frac{d}{l - X_{ymax}} \tag{3.8}$$

$$\alpha_2 = \sum_{x=0.9l}^{l} \frac{dy/dx}{l.N} \tag{3.9}$$

$$\alpha_3 = \sum_{x=0}^{0.1l} \frac{dy/dx}{l.N} \tag{3.10}$$

where N is the number of grid points used in CFD analysis, l is the length of aerostat envelope (in meters).

This approach to estimate the drag coefficient of an airship requires the information of slope of nose (bow) and tail (stern) ends. Not only that, a proper choice of parameters to obtain the C_{DV} is based on arbitrary selection, in other words, is not based on a scientific consideration [20]. Obviously, this method is not amenable to the multi-disciplinary optimization (MDO) approach and hence, cannot be used for the current attempt. Another empirical relation for C_{DV} obtained by combining Hoerner's empirical expression and the form drag equation is shown below. Hoerner's relation for Re $> 5 \times 10^6$ and practical level of surface roughness on the ship is as follows [1]:

$$C_f = \frac{0.043}{Re^{1/6}} \tag{3.11}$$

where C_f is the form drag and, also,

$$\frac{C_{DV}}{C_f} = 4(\frac{l}{d})^{\frac{1}{3}} + 6(\frac{d}{l})^{1.2} + 24(\frac{d}{l})^{2.7} \tag{3.12}$$

which upon combination yields the relation,

$$C_{DV} = \frac{0.172(l/d)^{1/3} + 0.252(d/l)^{1.2} + 1.032(d/l)^{2.7}}{Re^{1/6}} \tag{3.13}$$

where, l and d are the length and maximum diameter of the airship hull. The above equation is believed to give a reasonable estimate of the coefficient of drag for the present conditions [5][24][21].

The loss of momentum in the immediate vicinity (formally, known as the boundary layer) of the surface of the ship is associated with the drag force also known as skin friction drag. On the other hand, the form drag is a consequence of wake formation

at the rear of the body due to boundary layer separation [1]. Thus, it is interesting to study the effects of principal drag forces- the skin friction drag and the form drag, on the shape of the airship estimated by the empirical relation in eq. 3.13. From optimization point of view, a relatively lower skin friction drag or viscous drag results into minimum surface area, however, spherical shape (a shape with the lowest surface area) has a massive pressure or form drag in forward motion. A body is referred to as a bluff body if it has a predominant pressure drag as compared to viscous drag. On the other hand, it is referred to as streamlined when it exhibits a viscous drag domination. In this context, the reference optimization subject has a blunt nose and a relatively higher pressure drag due to the formation of airwake. Hence, it is regarded as a bluff body.

3.1.5 Material

The material of the envelope is to be decided in the design process factoring in elements like altitude of operation, endurance need, time of operation, and so on. For example, for stratospheric airships, the temperature is in the range of -56^o C, which could make the plastic coated film more brittle. In addition to that, the jointing techniques should be able to provide enough sustainable joint strength or load-bearing capability. At higher elevations, ultra-violet (UV) light rays are also a major cause of rapid degradation. Moreover, some of the other properties like emissivity, reflectivity, and absorptivity are also to be considered before the selection of material for the envelope. Porosity or gas retention component of an envelope material is another prime concern that has to be optimum for a given range of missions.

Keeping in mind the penalty associated with manufacturing, *polyester polyurethane* is chosen as the envelope material for the present design. It is heat sealable, flex fatigue resistant, and has good weatherability (on an average five-year life) [48]. It has a very low permeability, high crease resistance, and most importantly, joints are stronger than the material itself for it [1]. Polyester polyurethane offers high overall strength and stability [49]. The material acts as an excellent adhesive [49]. The

material selected has a thickness of 0.1016 *mm*. Owing to its qualities, this material is very widely used in airship manufacture [11][4][17].

3.1.6 Structure

The present subject, a semi-rigid airship, tends to combine the features of non-rigid airship and a rigid airship, essentially having a long lattice beam or a simple keel structure (for smaller airships) fixed at the bottom of the pressurized envelope. The keel aids in carrying the overall bending moment and also maintains the structural integrity of the ship. The model of the airship is shown in Fig. 3.1(a).

As can be seen, the gondola is enabled to slide freely on the keel and to control the CG of the ship as and when required. Notably, some of the most common shapes of Lighter-than-air (LTA) vehicles shapes reported in the literature are ellipsoidal, GNVR (a shape consisting of an ellipse, circle and parabola), lenticular, spherical and hybrid and so on [2] [4]. However, there are justifiable reasons for selecting the above shape i.e. it facilitates the sliding feature of the gondola, helps balance the

(a) Old airship model

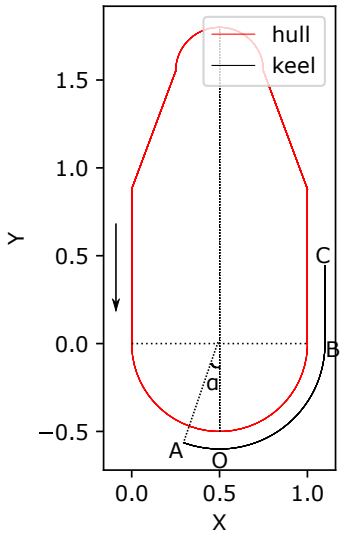

(b) New airship hull profile with keel: Gondola positions A, B and C

Figure 3.1: Structural modelling of semi-rigid airship: Old airship vs. new airship

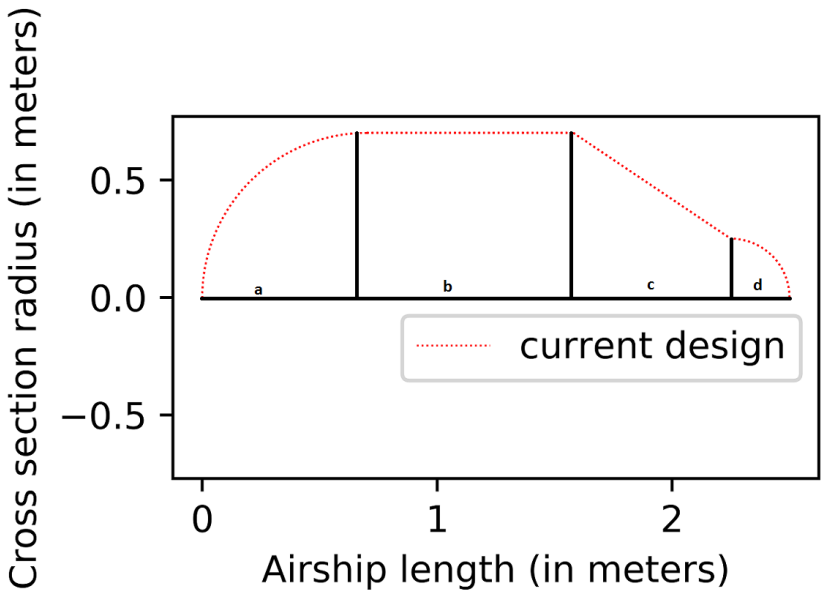

Figure 3.2: Airship body profile for the current design

total weight, and increases the maximum pitch angle.

Fig. 3.2 shows the body profile of the airship model that upon 360^0 revolution yields the hull of the ship. The geometry consists of four shape parameters namely, a, b, c, and d that also form the design vector for the routine. The optimization also incorporates an additional keel section at the aft of the hull as shown in Fig. 3.1(b). The length of the keel is from half-way through b to an angular extension of α above the nose-center.

Angle α

The keel is extended by an angle α over the nose to control the position of the CG with respect to the CV to design for rapid descent. Fig. 3.1(b) shows how at certain angle α, the CG of hull, keel and gondola unit are aligned on the longitudinal axis, thus, enabling 90^0 pitch. Gondola position along the rail at coordinates A, B and C are of interest for the CG consideration. Point C is at the mid-section of the straight portion (defined by variable b). The curved rail OB is defined by the variable a and the extension OA is estimated by the angle α. While attempting the perpendicular

descent, the gondola is at the position A and the value of angle α is computed for collinear CGs of all the components. When the three CGs lie on the same vertical axis, the effective CG of the vehicle will be on the vertical axis. As a result, the ship will experience perpendicular pitch, and also, the fastest descent. An in-built Python optimizer is used to solve for the value of α.

3.1.7 Envelope stress

Some of the pertinent work reported in the literature have incorporated circumferential stress as one of the objective terms [24] [15]. On the contrary, the current attempt employs a partially inflated hull and also, a minimized bending moment is realized due to the presence of keel that tends to support the weight of the airship. Consequently, envelope stress (circumferential and bending) is neglected in the optimization process.

3.1.8 Surface Area

The surface area (SA) contributes significantly to the total weight of the ship and, also to the payload capacity. Thus, in an effort to enhance the payload capacity of the ship, the surface area qualifies for a place in the objective function. The total surface area of the airship hull is the sum of the surface areas of individual geometric shapes in the mathematical model of the ship calculated as follows:

$$SA = 2\pi a^2 + 2\pi ab + \pi(a+b)\sqrt[2]{(a-d)^2 + c^2} + 2\pi d^2 \tag{3.14}$$

where, a, b, c and d are the independent variables representing the dimensions for the body profile.

3.1.9 Relation between buoyancy and gross weight

The current work aims to maintain the equality relation between gross weight and the static lift for the MDO routine, where the total weight of the airship is given by-

$$W = m_t \times g = (m_e + m_{gas} + m_g + m_b + m_r) \times g \tag{3.15}$$

where m_e is the mass of the envelope, m_{gas} is the mass of helium gas, m_g is the mass of gondola, m_b is the mass of ballast, and m_r is the total mass of the keel. Also, the buoyancy or static lift of the airship for a given shape is given as [1]:

$$B = (\rho_a - \rho_{gas})V \times g \tag{3.16}$$

where ρ_a is the density of air, ρ_{gas} is the density of helium gas, V is the volume of the hull and g is the gravitational acceleration.

The volume of the hull is given by

$$V = \frac{2}{3}\pi a^3 + \pi a^2 h + \frac{\pi}{3}h(a^2 + d^2 + ad) + \frac{2}{3}\pi d^3 \tag{3.17}$$

3.1.10 Centre of gravity

Due to the state-symmetric shape of airship hull, the fundamental theory of center of gravity of a 2D shape is used to formulate the expression for the value of α. The rail has negligible thickness and is accordingly modeled as a 2D shape. The expression for the CG of the airship to be on the vertically centered line (x axis) obtained is as follows:

$$\left(\frac{2b + acos\alpha}{b + a\pi + 2\alpha a}\right)\left(\frac{b + \pi a + 2\alpha a}{4}\right)m_r = m_g sin\alpha \tag{3.18}$$

where a, b, c, and d are the design variables, m_r and m_g are the masses of rail and gondola respectively.

Chapter 4

Optimization set up

This chapter focuses on the optimization approach and the simulation set up for the current multi-objective optimization (MOOP). The objective of the present effort is to develop an optimization algorithm routine in order to optimize the airship hull. In the present research, hybridization of algorithms is achieved by combining a global stochastic heuristic (genetic algorithm) and a local stochastic heuristic (hill climbing) to achieve improved performance.

4.1 Formulation of the multi-objective function

The objective function for the optimization process is based on aerodynamic and weight-optimum design for a given user-defined payload requirement. It is customary to introduce the constraints in a multi-objective optimization (MOOP) function by adding an equivalent penalty in the function itself, thereby making it unconstrained in nature [25] [26] [24] [5]. The complete fitness or objective function to be minimized is defined as follows:

$$\text{minimize } F_{comp} = w_1 \frac{C_{DV}}{C_{DV0}} + w_2 \frac{SA}{SA_0} + w_3 \frac{m_r}{m_{r0}} + w_4 \frac{\kappa}{\kappa_0} \tag{4.1}$$

where C_{DV} is the volumetric drag coefficient of the airship hull, SA is the surface area of the hull, m_r is the mass of the keel and, κ refers to the square of the difference between the buoyancy (B) and the total weight (W) of the airship. Also, the term kappa

$$\kappa = (W - B)^2 \tag{4.2}$$

and,

$$\sum_{i=1}^{n} w_i = 1 \tag{4.3}$$

The reference design is the subject of the optimization process. It corresponds approximately to the volume needed to lift the requested payload i.e. 500 g. Also, it has

dimensions that roughly compare to the design already available in the laboratory. Additionally, C_{DV0}, SA_0, m_{r0} and, κ_0 correspond to the reference design while their respective numerators correspond to the iterative design parameters that are also a function of the design variables. w_1, w_2, w_3, and w_4 are the weight constants to be factored to different objective terms.

The third term in the objective function keeps a check on the length of the keel. Especially, the term κ is significant to keep the total volume to the minimum in optimization. It facilitates to filter the infeasible solutions i.e. volumes that correspond to lower buoyancy than required; and volume that has too high buoyancy than required. This is essentially achieved by applying a severe penalty, that is changing quadratically to the deviation from neutral, to such shapes.

4.2 Optimization approach

In the beginning of the routine, it takes in the initial design vector based on the reference design to compute the value of α. The term α is a function of the design variables a, b, c and d. The in-built python optimizer is used to solve for the value of this angular extension at the aft of the ship. This value of α is subsequently passed on along with other input parameters including lower and upper bounds for the design variables to the hybrid GA operators for optimization of the parametric objective function. In addition to that, the flight conditions are fed to the optimization routine that begins the exploration and exploitation of the search space as expected in evolutionary algorithms. Eventually, the algorithm outputs the best result after the converging criteria is met i.e. the number of generations is reached, as can be seen in the flowchart summary in Fig. 4.1.

The table 4.1 shows the value of input parameters such as weights for the different objective functions and masses (gondola, ballast, rail, fins, and fabric) seeded into the optimization algorithm. All these parameters are supplied by the user based on

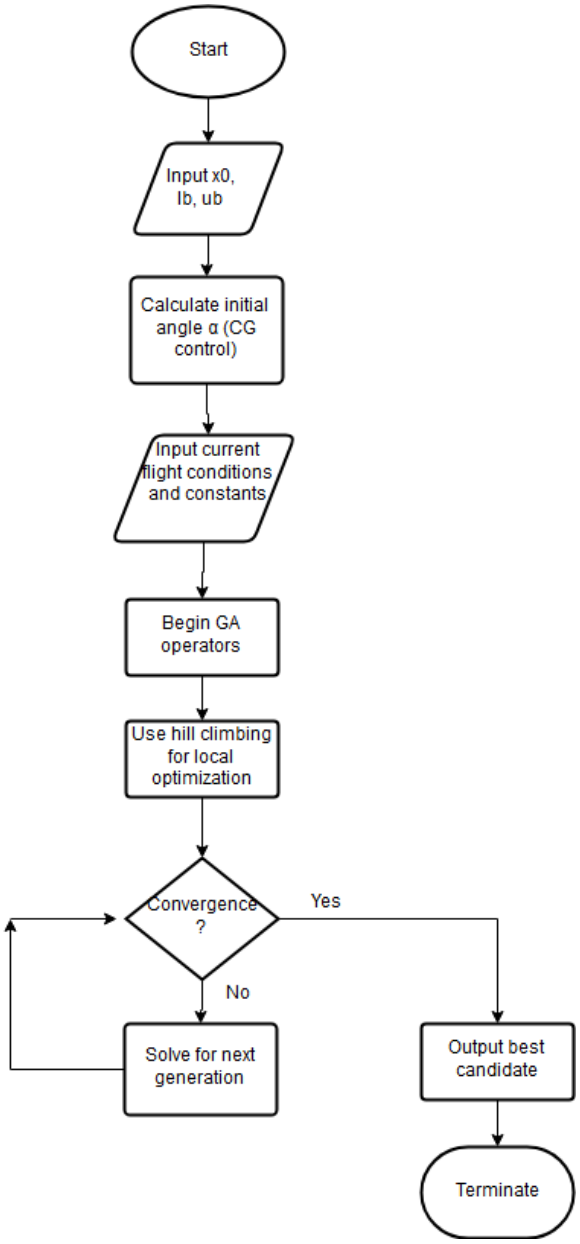

Figure 4.1: Design methodology flowchart

Table 4.1: Input Parameters

Parameter	Value
w_1	0.2
w_2	0.4
w_3	0.1
w_4	0.3
m_g	0.5 kg
m_b	0.2 kg
m_{ru}	0.1 kg
m_f	0.032 kg
ρ_{fab}	0.225 kg/m^2

the flight objectives.

GA is inherently a stochastic optimization process that is based on generating designs from random number generation. Therefore, the algorithm will inherently generate different design solutions for the same problem. That being said, all the generated solutions will be optimal solutions given the constraint settings and variable bounds. To remedy this, it is recommended to run the simulation multiple times for the same problem to gauge the best possible solution and evaluate the results to obtain the best solution [28].

4.3 Implementation details of the algorithm

Recent developments in the GA implementation indicate the algorithm superiority upon hybridization with a local minimizer. In GA, the quality of the solution cannot be evaluated due to the random nature of the solution and lack of knowledge. Thus, the reinforcement of GA mutation with a local mutation based on reinforcement learning is a refinement to the overall performance [50]. It is a recommended practice to employ a non-deterministic hill climbing into the hybridization process [51]. GA when combined with hill climbing, is also reported as memetic algorithm (MA) in the literature [52] [53]. Owing to the nature of problem i.e. multi-variable, multi-modal, constrained, and non-linear optimization model, the various operators of the

non-traditional evolutionary GA are explained as follows:

4.3.1 Encoding, precision, and limits

- Encoding: Since the search space is continuous in nature, real-value encoding is employed to express the values of variables. For instance, the initial solution is expressed as:

$$x_0 = [0.7 \quad 0.88 \quad 0.67 \quad 0.25] \quad \text{in meters} \tag{4.4}$$

  where x_0 is the initial design vector comprised of bow radius, length of constant diameter mid-section, length of rear cone and, radius of the stern corresponding to the reference shape. The numerical values shown in equation 4.4 correspond to the reference shape used in the initialization of the algorithm.

- Precision: In the continuous GA, the precision of the digital computer is limited by the internal machine precision and round-off. Thus, the machine round-off error defines the precision of the algorithm. In our case, the computer uses 16 bytes for each number in decimal form. In other words, a number is represented by a maximum of 16 digits, and thus, a precision of 16 decimal digits.

- Limits: On account of the fact that GA is inherently a search technique, it is vital to limit the exploratory effort by limiting the region of search space. Quite commonly, this is achieved by either bounding the variables of the problem or by enhancing the diversity in the initial population which, in turn, helps widening the focus on the region of interest [29] [51]. Given the nature of the problem i.e. believed to be multi-modal, the former technique is employed and the bounds on the variables are as follows:

$$\text{Lower bounds} = [0.70 \quad 0.70 \quad 0.70 \quad 0.20] \tag{4.5}$$

$$\text{Upper bounds} = [3.0 \quad 2.00 \quad 3.0 \quad 0.25] \tag{4.6}$$

The bounds roughly correspond to minimum and maximum volumes for supporting the range of payloads 250 g and 1 kg. Additionally, the variable 'd' is intentionally kept

lower as compared to other independent variables in agreement with the aerodynamic effect. It is also taken into consideration that an MOOP needs enough breathing interval between the variable limits to optimize the objective function.

4.3.2 Initial population - a set of feasible solutions

A summarized flowchart of the HGA algorithm is shown in Fig. 4.2 to illustrate the steps in the algorithm. Following the initialization of the optimization, GA proceeds with an initial set of population that is progressively improved over the number of iterations. Evidently, the population matrix is of the order $N\times$ 4, where N is the number of individuals in the pool which is set to be 20. These array of continuous values (unnormalized), uniformly spread within the bounds, is generated randomly using an unbiased random number generator. Subsequently, the relative worth of each individual is computed using the fitness vector of size $N \times 1$.

4.3.3 Natural Selection

In this step, a decision is made to allow some of the members of the population, understandably by the virtue of their fitness, to reproduce while the others are discarded to make room for the new off-springs. Following a rule of thumb, a rate of selection of 50% is employed for the problem [29]. Such a high selection rate means the half of the population is overhauled every generation. Quite notably, this process has a tremendous impact on the improvement of mean fitness of the population over the number of generations. Consequently, the average fitness of the population is greatly reduced after a few iterations.

4.3.4 Pairing

The selected parents are paired randomly based on the probabilities of selection. This roulette-wheel pairing computes chances of selection on the basis of fitness of the individual. For instance, all the individuals are ordered by decreasing fitness. Also, the cumulative probability of each individual is calculated as shown in table

4.2. Now, to pick the parents, as many random numbers are generated. For example, let's suppose, the generated random numbers are (0.784, 0.4141) and (0.2321, 0.998) for picking two parents. Then, the set of chromosomes to be selected is given by the vectors:

$$xy = [3 \quad 2] \tag{4.7}$$

$$xx = [2 \quad 4] \tag{4.8}$$

The numbers in the vectors are obtained in the way that 0.784 is the highest number less than the cumulative probability till chromosome 3 and so on. Besides, the mating occurs such that chromosome 3 mates with chromosome 2 and chromosome 2 pairs with chromosome 4 to produce two off-springs each.

4.3.5 Crossover

After pairing i.e. once the parents are shortlisted for the reproduction, a suitable crossover strategy is employed. Some of the most common crossover strategies for a continuous GA are uniform crossover, blending crossover, quadratic crossover, heuristic crossover, linear crossover and so on [29]. Out of all these, blending method of mating is considered effective for a continuous GA with four variables [29]. In this method, the mixing parameter β is used to modify the offspring genes. The crossover points are also generated randomly. For instance, let's say, the crossover point is 2 (generated randomly) and β comes out to be 0.5444 (also generated randomly) for parents *P1* and *P2*. Then,

$$P1 = [x_1 \quad x_2 \quad x_3 \quad x_4] \tag{4.9}$$

Table 4.2: Rank Weighting

Chromosome	Gene x	Gene y	Probability	Cumulative Probability
1	7.7246	5.5655	0.4	0.4
2	0.1887	8.9214	0.3	0.7
3	2.3434	6.2332	0.2	0.9
4	5.3433	0.1233	0.1	1.0

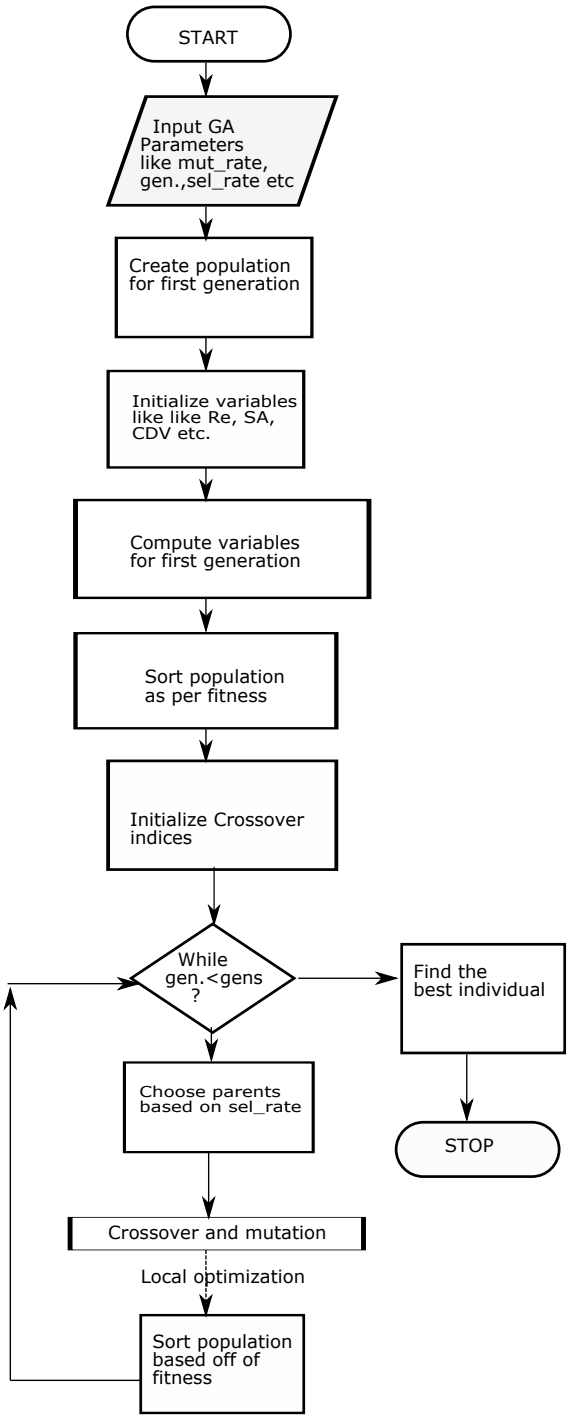

Figure 4.2: GA flowchart

$$P2 = [y_1 \quad y_2 \quad y_3 \quad y_4] \tag{4.10}$$

$$x_2^{new} = x_2 - \beta[x_2 - y_2] \tag{4.11}$$

$$y_2^{new} = y_2 + \beta[x_2 - y_2] \tag{4.12}$$

where, x_2^{new} and y_2^{new} are the modified variables for the off-springs. This method provides the advantage of obtaining the values of variables exclusive to that of the parents, thus, introducing new genetic content in the population. Here, the offsprings are given by c_1 and c_2 such that,

$$c_1 = [x_1 \quad x_2^{new} \quad x_3 \quad x_4] \tag{4.13}$$

$$c_2 = [y_1 \quad y_2^{new} \quad y_3 \quad y_4] \tag{4.14}$$

4.3.6 Mutation

It is indispensable to introduce a sufficient quantity of new information in the population in an effort to avoid premature convergence [54]. Mutation is a classic technique to accomplish the function that also confirms to the biological process in nature. In the present context, mutation refers to the alteration of certain number of gene (variable) values from its initial state [14]. For the present approach, a mutation probability of 10% is employed based on a rule of thumb as described in [29]. Nevertheless, a sensitivity analysis for the mutation rate is performed and is reported in Chapter 5. The mutated variables are replaced by random numbers within the bounds for the corresponding variables.

4.3.7 Hill climbing

In an unconventional sense to the simple GA (SGA), a local optimization is attempted on the mutated population for every iteration. This effort to hybridize the regular GA is effective and is feasible to implement for a problem of this scale (i.e. with four variables) as demonstrated by numerous researchers [52] [53] [33]. The flowchart as shown in Fig. 4.3 highlights the significant steps in the local tuning of the variables

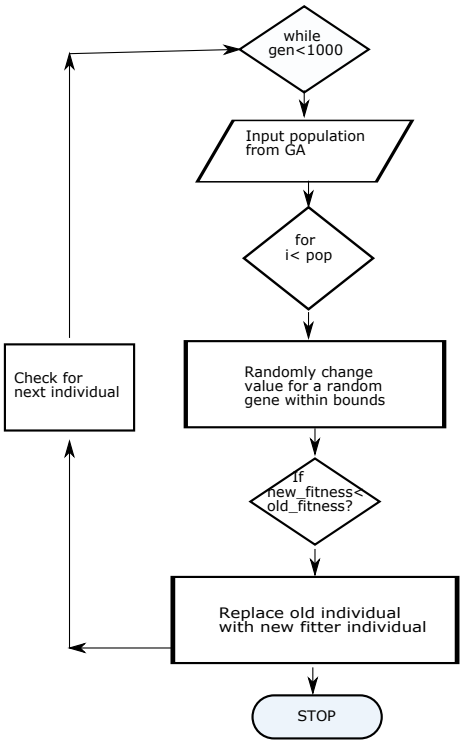

Figure 4.3: Hill climbing flowchart

in hill climbing. Post mutation, all the individuals of the population pool tend to shift to a better neighborhood until the convergence criteria is met.

4.3.8 Convergence criteria

The routine could be stopped once a set of acceptable solutions is obtained or once the set number of generations is exceeded [29]. The latter technique is employed here keeping in mind the solutions will never be all same or even close enough to converge provided a mutation is performed at every iteration. The convergence figures including the number of iterations/generations of GA and of hill climbing are specified in table 4.3. As can be seen in the flowchart 4.2, the algorithm terminates once the set limit on the number of generations (gens.) is reached.

4.4 Benchmarking the algorithm

In algorithmic optimization, it is customary to benchmark the developed routine against a test function with the details of computer configuration in order to analyze its efficiency [54] [51] [28]. Typically, the test function has plethora of local minima spread over the search space, is non-convex, multi-modal, and multi-variable [54]. For the present research, the two-variable Rastrigin's function is chosen to be the test subject. Besides, the simulations were performed on Intel(R) Core(TM)-i5-4590 CPU 3.30 GHz processor with a RAM of 4 Gigabytes. The topography of the function is illustrated in the Fig. 4.4, and it is expressed as:

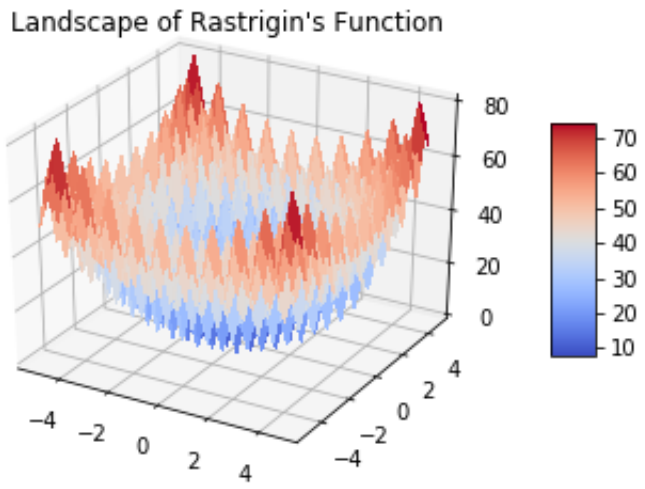

Figure 4.4: Design space of Rastrigin's function

Table 4.3: HGA Input Parameters

Parameter	Value
Population	20
selection rate	0.5
mutation rate	0.1
generation-GA	50
generations-HC	1000

$$F(x) = Ad + \sum_{i=1}^{n}[x_i^2 - Acos(2\pi x_i)] \tag{4.15}$$

where A= 10 and d is the number of dimensions/variables. Therefore, for a two-dimensional space, the expression is given by:

$$F(x) = 20 + x_1^2 + x_2^2 - 10(cos2\pi x_1 + cos2\pi x_2) \tag{4.16}$$

The test function has only one global minimum, that is, at the origin (0, 0), where the value of the function is 0. Also, the farther the local minimum is from the global minimum, larger is the value of the function. The results for the benchmarking of the algorithm are summarized in table 4.4. The hybrid GA was set for convergence at 50 generations for the GA and 1000 generations for the hill climbing. Despite such complicated search space, the algorithm was observed to solve for the global minimum in 10 seconds. Evidently, the HGA is superior to normal GA in regards to precision and computer time.

Ergo, it can be concluded that the routine is robust and efficient to locate the global optimum even in a complicated landscape as is for the test function.

4.5 Optimization engine- Pareto GA

It is customary to solve multi-objective optimization problems by formulating a series of single objective problems which are solved by a single optimization routine also called as optimization engine [28]. In the present research, tournament selection

Table 4.4: Benchmark test results for the HGA

Test	**Optimum candidate**		**F(x)**
	x_1	x_2	
hybrid GA	$1.00494249 \times 10^{-10}$	$1.24710245 \times 10^{-09}$	0
analytical solution	0	0	0

technique is employed for obtaining designs that are used over the generations in the routine. The principal advantage of this method is that it circumvents the idea of fitness of a design. Instead, it gives the distribution of the objectives in the criterion space, thereby, enabling the user to make a better decision in scaling weights to the objectives. Some of the other prominent methods listed in the literature are: niche technique, elitist strategy, Pareto-set filter and so on [27]. A detailed flow chart for the Pareto optimization routine is shown in Fig. 4.5. The algorithm was run for the three objective functions as shown:

$$\min F_1 = \frac{C_{DV}}{C_{DV0}} \tag{4.17}$$

$$\min F_2 = \frac{SA}{SA_0} \tag{4.18}$$

$$\min F_3 = \frac{m_r}{m_{r0}} \tag{4.19}$$

and the constraint (neutral buoyancy) is employed at the post convergence step to eliminate all the infeasible design solutions. The bounds on the values of the design variables is kept identical to the previous optimization approach (i.e. 'Sum of weighted functions').

The Pareto GA algorithm is seeded the values of gondola mass, rail mass per unit length (m_{ru}), ballast mass to maintain the same airship configuration as for the 'sum of weighted functions' approach. As per the parameter settings, the neutral buoyancy constraint helps generate design solutions that have sufficient buoyancy to sustain the payload of 500 *grams*. Fig. 4.5 summarizes the key components of the Pareto GA algorithm. In the beginning, the algorithm works with three objective functions- the surface area (SA), the coefficient of drag (C_{DV}) and the mass of rail (m_r). However, the Pareto GA algorithm could be employed for higher number of complementing objectives. Quite evidently, Pareto GA needs a large population size to work well in order to generate a precise curve at the Pareto front. As a result, tournament selection is employed in the process. It is a common procedure to normalize the values of fitness for different objective functions [28][18]. The population size for the algorithm

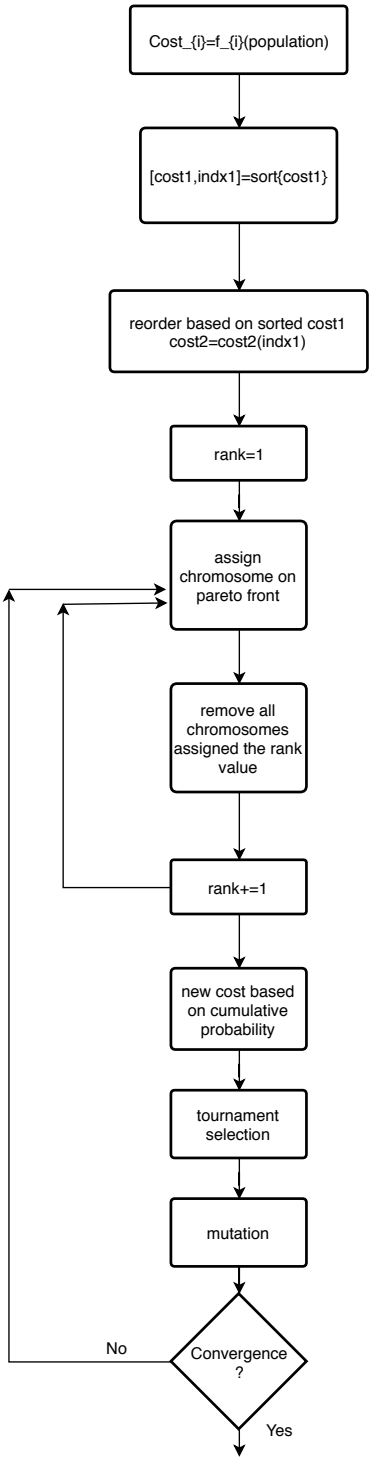

Figure 4.5: Pareto GA flowchart [29]

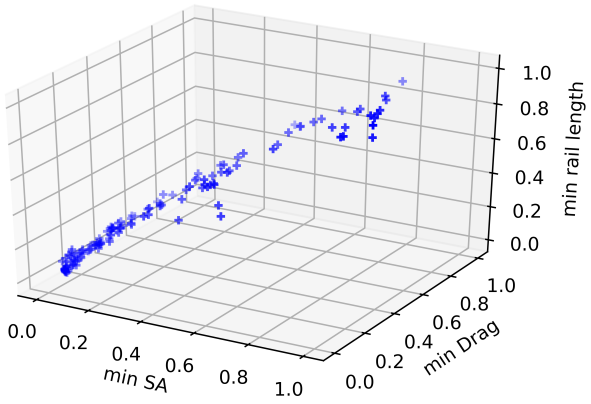

Figure 4.6: Final population distribution

is chosen to be 250 with a selection rate of 50%, mutation rate of 10%.

Fig. 4.6 shows the final population obtained after the Pareto optimization. The three objectives are along the three axes- SA, C_{DV} and m_r. As can be observed, the GA provides a reasonable approximation to the Pareto optimal solutions. It can be observed from the final 3D plot in Fig. 4.6 that the final population consists of most of the individuals along the lowest strata of the value of individual objectives (at or near zero). This phenomenon is in accordance with the nature of the GA i.e. optimizing the average fitness of the population. A suitable design solution according to a user requirements could be picked from the available optimized population.

Chapter 5

Simulation results and discussion

In this chapter, the application of the developed HGA code to the design optimization of rapid-descent airships of various payload carrying capabilities is discussed. A short note on the mass distribution of the optimum design and the reference design is also included to understand the implications of optimization on different components of the airship, and the sensitivity of various important parameters is presented. Lastly, to establish the credibility to the choice of objectives and other optimization characteristics, the results are presented in reference to a commercially available off-the-shelf airship product.

5.1 Results

The plot in Fig. 5.1 for the fitness trend shows the comparison of the best fitness (i.e. objective function value of the optimum for a generation) to the mean fitness of the population over the number of iterations for the complete objective function shown below:

$$\min F_{comp} = \left(w_1 \frac{C_{DV}}{C_{DV0}} + w_2 \frac{SA}{SA_0} + w_3 \frac{m_r}{m_{r0}} + w_4 \frac{\kappa}{\kappa_0}\right) \times 100 \tag{5.1}$$

Here, the complete function is designed to have a payload capacity of 500 g. The lower and upper bounds on the design variables is as shown in Chapter 4. The objective function is optimized subject to the constraint that all the output designs are neutrally buoyant.

It can be observed that the maximum fitness at the start of routine is at 100%. At the same time, the mean fitness is quite over 100% owing to the overwhelming number of non-optimum individuals who have fitness far off from the best candidate at any instant of time. Moreover, it is noticeable that the value of the objective function for all the individuals in the population pool plummets only after a few iterations. This

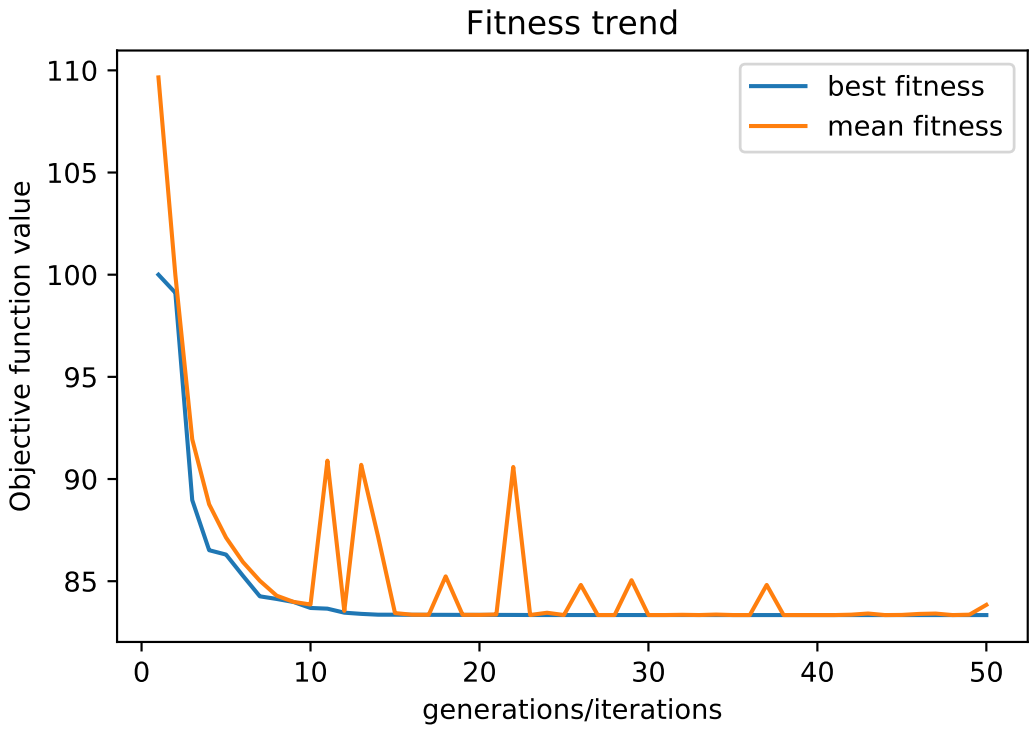

Figure 5.1: Fitness trend

Table 5.1: Input Parameters

Parameter	**Value**
w_1	0.2
w_2	0.4
w_3	0.1
w_4	0.3
m_g	0.5 kg
m_b	0.2 kg
m_{ru}	0.1 kg
m_f	0.032 kg
ρ_{fab}	0.225 kg/m^2

action of tremendous improvement (more than 15%) in the fitness of the population is ascribed to the fast convergence capabilities of HGA. The abrupt spikes in the mean fitness profile reflect the occasional introduction of new individuals in the population by mutation. Also, it is imperative to avoid mutation of the elite individual in the population [29], thus, the process of elitism makes sure that the best individual is not lost in any generation. The plot accentuates how the mean fitness tends to fall in line with the best fitness except for the intermittent mutations. Evidently, GA is earmarked for improving the entire population pool and not just one or a few individuals [29]. The computation time for the complete objective function was just 18 seconds. The time taken is a little higher than that of the benchmark test function on account of the number of variables involved in the objective function. Therefore, it can be said that the process is computationally effective albeit the efficiency is dependent on the size and dimensions of the search space.

The weight coefficient w_4 is chosen in a manner such that the total structural weight is balanced with respect to the total buoyancy. All other weights for the objectives are based on engineering decisions and can also be user-defined for a given range of missions.

5.1.1 Optimization model variants

Other than the complete objective function, the algorithm was simulated for two variants of the objective function using different weights ($w_1 = w_2 = 0.5$) for volumetric drag and κ called as '*drag model*' F_{drag} as shown in eq. 5.1 and, for surface area and κ called as '*surface area model*' F_{SA} as shown in eq. 5.2, respectively:

$$\min F_{draf} = \left(w_1 \frac{C_{DV}}{C_{DV0}} + w_2 \frac{\kappa}{\kappa_0}\right) \times 100 \tag{5.2}$$

$$\min F_{SA} = \left(w_1 \frac{SA}{SA_0} + w_2 \frac{\kappa}{\kappa_0}\right) \times 100 \tag{5.3}$$

The purpose of devising these optimization models is to appreciate the conflicting nature of the objectives and to optimize the vehicle for minimum drag and minimum

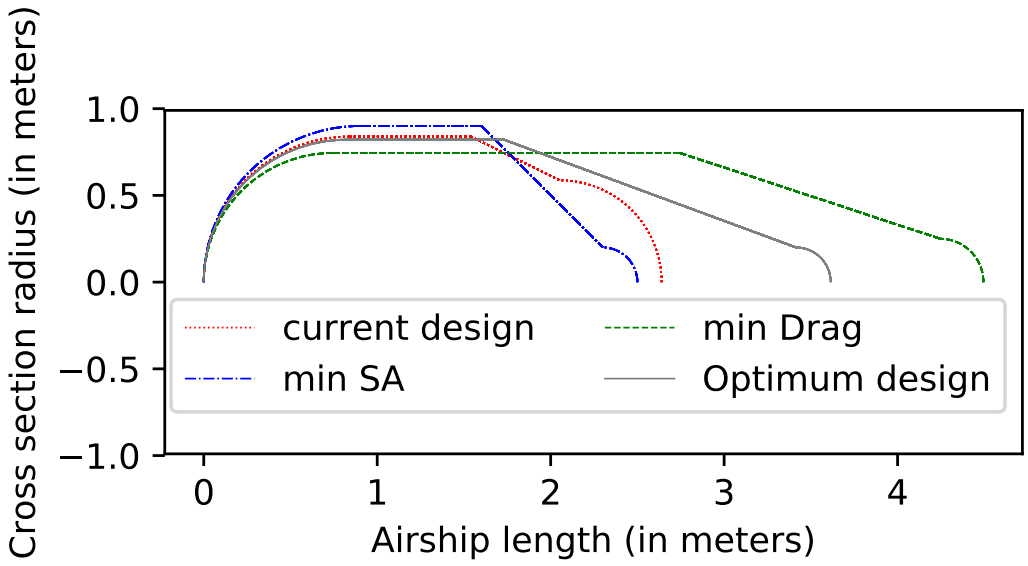

Figure 5.2: Body profile comparison with different weights

mass, that is also quite intuitive. Fig. 5.2 shows the body profile for different models compared to the reference profile. As can be seen, the 'SA model' tries to decrease the surface area by assuming a spherical shape while the 'drag model' tends to make the shape more streamlined by increasing the length of the airship. At the same time, the optimum design profile tries to strike a balance of several factors combined and achieves the optimum design.

To appreciate the effect of aerodynamics on the shape of the profiles achieved by simulation, the skin friction drag results in a shape that has the least total surface area for the same surface finish while the form drag governs the streamlining of the rear of the ship [1].

In Fig. 5.2, it is also noticeable that the aft of the ship tends to attain the minimum radius in comparison to that of the red-curve of the reference design. It is to be noted that the C_{DV} is a non-dimensionalized quantity for the total drag coefficient (i.e. it accounts for all types of drag like form drag, skin friction drag and so on). Using the fundamentals of aerodynamics, the phenomenon could be attributed to the fact that beyond the point of transition from laminar to turbulent, the wetted surface

Table 5.2: Comparison of design properties for different profiles

Property	Reference design	Optimum design	min-SA	min-Drag
Surface area (m^2)	12.847	14.9365	12.7212	18.1769
Drag coefficient	0.07523	0.05155	0.0899	0.0434
Volume (m^3)	4.04137	4.65	4.08121	5.6476
Reynold's number	417631.92	408460	447824.7	370631.85
Mass of rail (kg)	0.1868	0.194	0.1978	0.234754

area attempts to get smaller in order to minimize the skin friction drag [22]. The effect seems to be pronounced for the LTA ships on account of the fact that due to larger surface area of airships the skin friction drag is the principal drag [1]. Also, the structural feature of an axisymmetric body about the line of flight is a justified choice owing to the fact that it experiences the least form drag [1]. Needless to mention, the sharp edges in the simplified airship body profile due to discontinuity between different geometric shapes lead to manufacturing and operational penalties. Thus, a suitable fillet is introduced while building the hull to mitigate the issue.

The bar chart shown in Fig. 5.3 tries to capture the characteristics of the design outcomes from the simulation. It highlights the improvement in the design features like objective function value, aerodynamic drag, SA, volume, and the mass of keel (m_r) for the three simulation models.

$$\text{Improvement in Fitness} = \frac{\text{optimum/best fitness}}{\text{reference fitness}} \times 100 \tag{5.4}$$

$$\text{Improvement in drag} = \frac{\text{optimum drag}}{\text{reference drag}} \times 100 \tag{5.5}$$

$$\text{Improvement in SA} = \frac{\text{optimum SA}}{\text{reference SA}} \times 100 \tag{5.6}$$

$$\text{Improvement in Volume} = \frac{\text{optimum V}}{\text{reference V}} \times 100 \tag{5.7}$$

$$\text{Improvement in mass of rail} = \frac{\text{optimum } m_r}{\text{reference } m_r} \times 100 \tag{5.8}$$

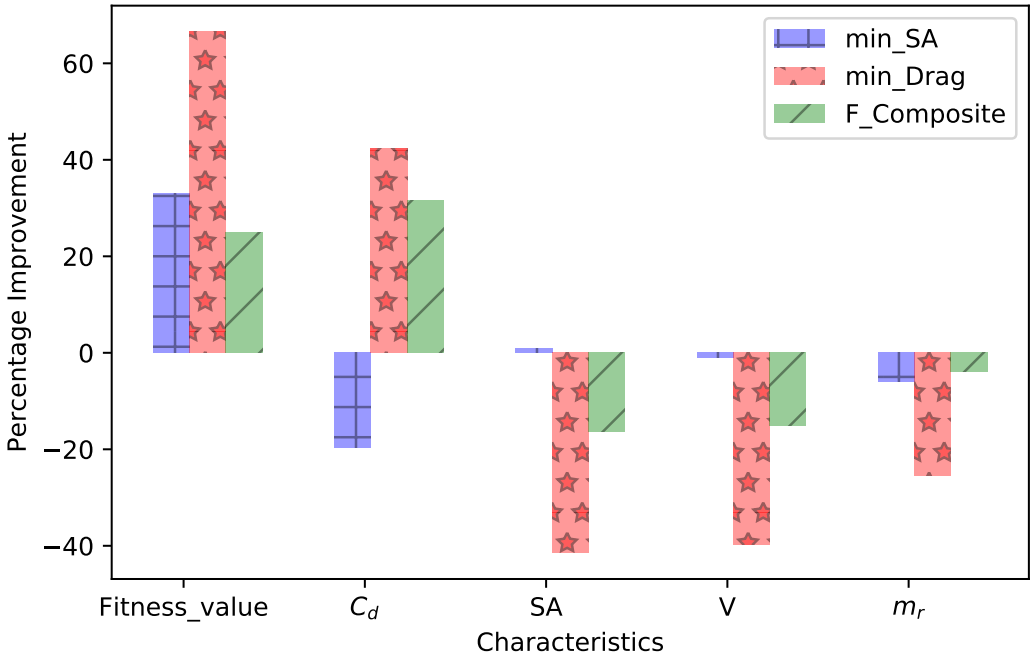

Figure 5.3: Improvement in the design with respect to reference design

Here, negative values of equations 5.4 to 5.8 indicate an improvement in the design relative to the reference shape labeled as 'current design' in Fig. 5.1. Notably, the improvement in fitness for the drag is maximum but it does not consider the structural component (surface area) and, hence, cannot be a preferred design. Likewise, the model for minimum envelope area is not preferable because it experiences relatively significant drag. The bar plot for surface area and the drag characteristics is very intuitive whilst the trend for the volume requirement for the min-drag model experiences a very logical but dramatic increment despite the fact that the aft end is very narrow. Lastly, the mass of rail which is a function of radius at the bow and the length 'b' of the cylindrical portion, is evidently optimized for the complete objective function.

A detailed list of data is put together in table 5.2 to give the reader a perspective into the design output. Additionally, using the values from the optimized design, the mass distribution for reference airship and optimized airship are shown in the pie charts in Fig. 5.4. As expected, the envelope has a significant contribution to the total

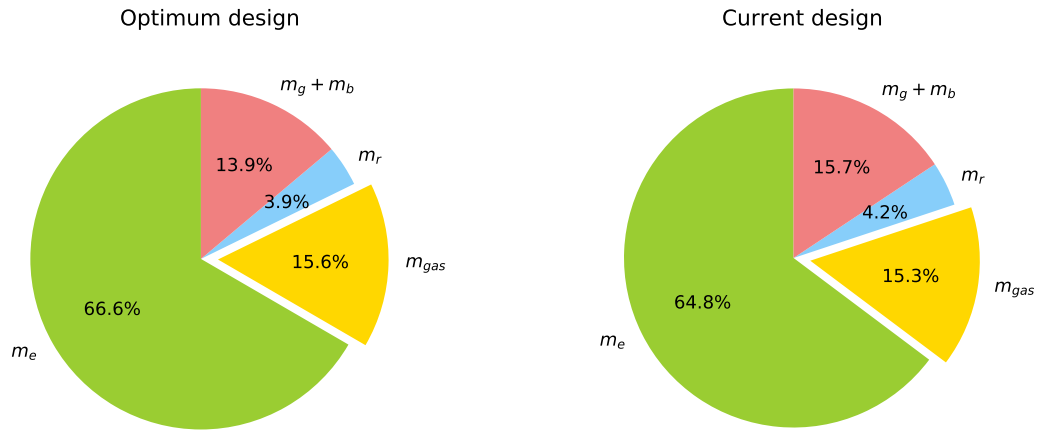

Figure 5.4: Mass distribution

weight, in most cases being almost a two-third of the total weight. On the contrary, it is counter-intuitive that the mass of the lifting gas and the gondola and the ballast mass are comparable. The weight contribution of rail is optimized considerably due to use of a carbon fiber material. In addition, the algorithm optimizes the size of rail because of the penalty imposed by mass of rail in the complete objective function.

5.2 Sensitivity analysis

In this section, sensitivity of various parameters like objective function (fitness) and payload is measured with respect to the design variables and the volume of the airship, respectively.

The algorithm was tested for a total of five different gondola masses and the results are plotted to scale. As expected, Fig. 5.5 shows how an increase in the mass of gondola (m_g) causes a linear increase in the total buoyancy required to compensate for the extra weight.

In Figs. 5.6, 5.7, 5.8, 5.9, the sensitivity of the complete objective function with respect to the independent design variables is captured. The study was performed by keeping all the other variables constant at their optimized values while the subject gene varies within their limits. In Fig. 5.6, it can be seen that there is a benign

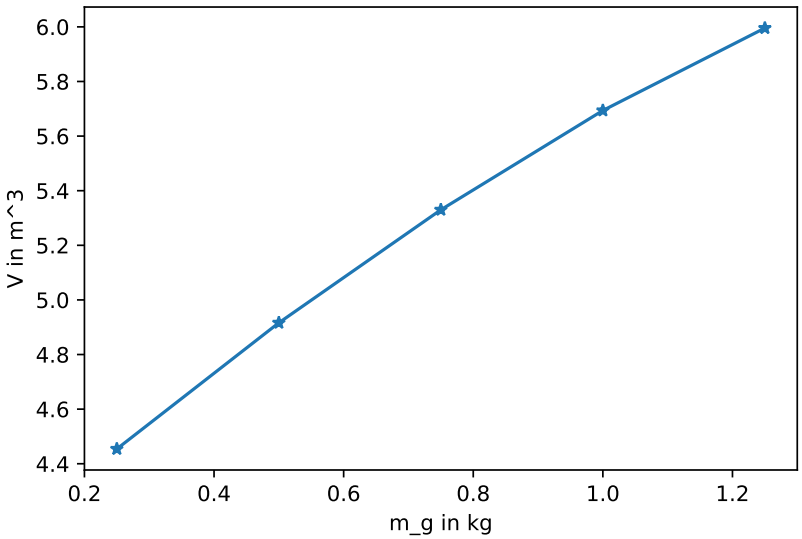

Figure 5.5: Volume vs. Payload plot

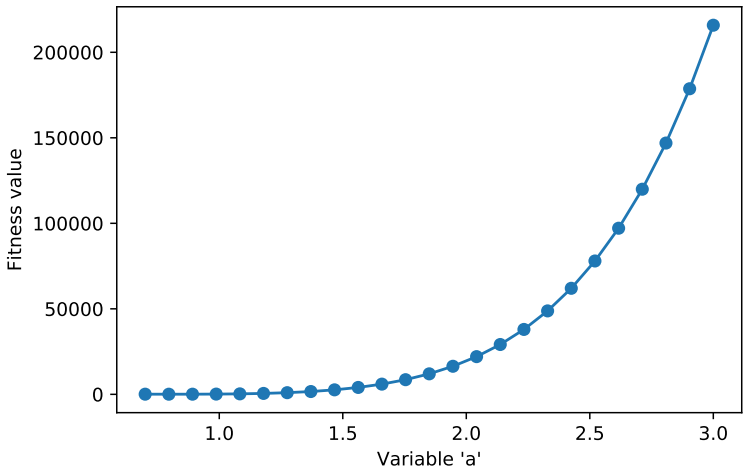

Figure 5.6: Fitness vs ‘a’

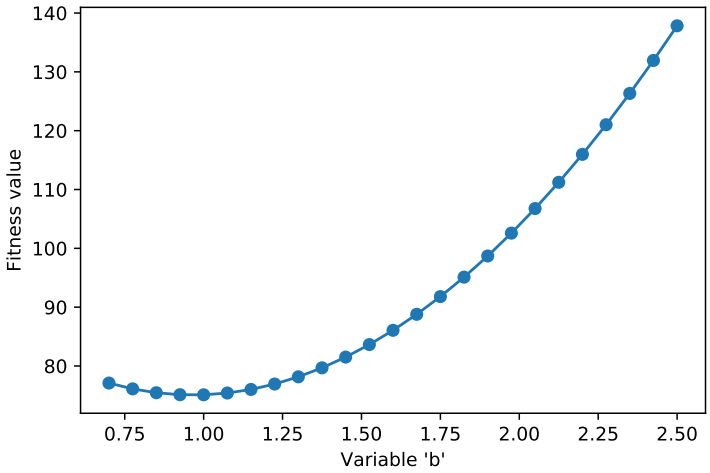

Figure 5.7: Fitness vs 'b'

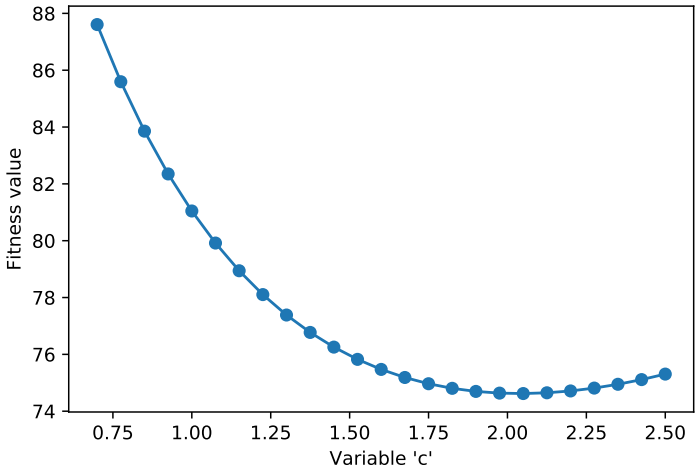

Figure 5.8: Fitness vs 'c'

region in the whole interval i.e. (0.7-3 m) for the variable 'a' to affect the fitness. On the other hand, there is a narrow valley that is favorable for the minimization of the fitness as seen in Fig. 5.7. This region is around 0.9-1.2 m of the dimension 'b'. Similarly, Figs. 5.8 and 5.9, highlight the dependencies of the fitness on the variables. It is interesting to note that the variable 'c' has a crucial effect on the design as it increases. But, like other variables it has a regional optimality. This can be understood by the fact the after a certain limit, the portion becomes too heavy due to conical shape of the stern as it has a higher surface area but a lower buoyancy.

Although the plots in Figs. 5.6, 5.7, 5.8, 5.9 give a reasonable estimate of the effects

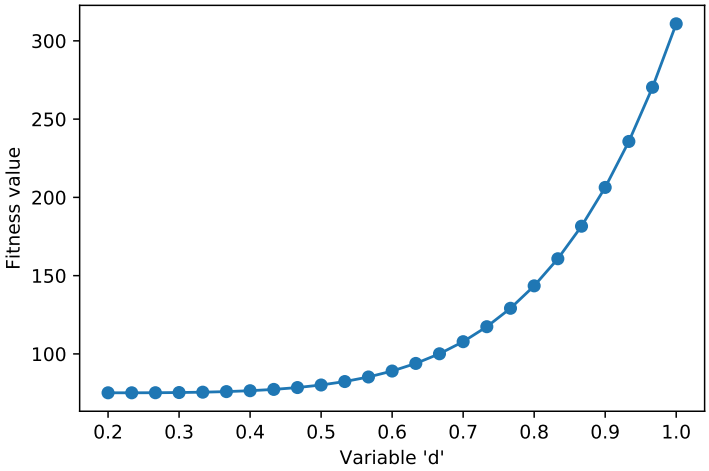

Figure 5.9: Fitness vs 'd'

of the variables on the parameters, they do not take into account the relation between the variables themselves. For example, an increase in the value of variable 'a' causes a gain in volume and buoyancy, however, it also affects the fitness due to larger keel length around the nose. In other words, 'b' is a better candidate to enhance the buoyancy as it has a smaller factor of keel attached to it. The algorithm tries to locate the global minimum by targeting the optimum regions for several variables simultaneously. It is the novelty of the algorithm to give optimum solutions every time the routine is run.

Finding optimal values of mutation and selection rates is significant to improve the performance of a GA [55]. In Fig. 5.10, the sensitivity of the best-fitness (fitness of optimal solution) apportioned to the mutation rate and selection rate is indicated by blue and orange curves, respectively. Selection rates are the probability measure of rate at which individuals are subject to crossover. Typically accepted range of values of selection rate is 0.5 (half of the population mates) to 1 (entire population mates) for a continuous GA [56]. A direct consequence of higher selection rate is that the new solutions will be introduced relatively quickly. Moreover, if the rate of selection is very high, it essentially starts serving the task of mutation, a secondary operator to restore genetic content, as no elite member is protected each generation. The analysis for the present problem shows that 0.5 is the rate at which the value

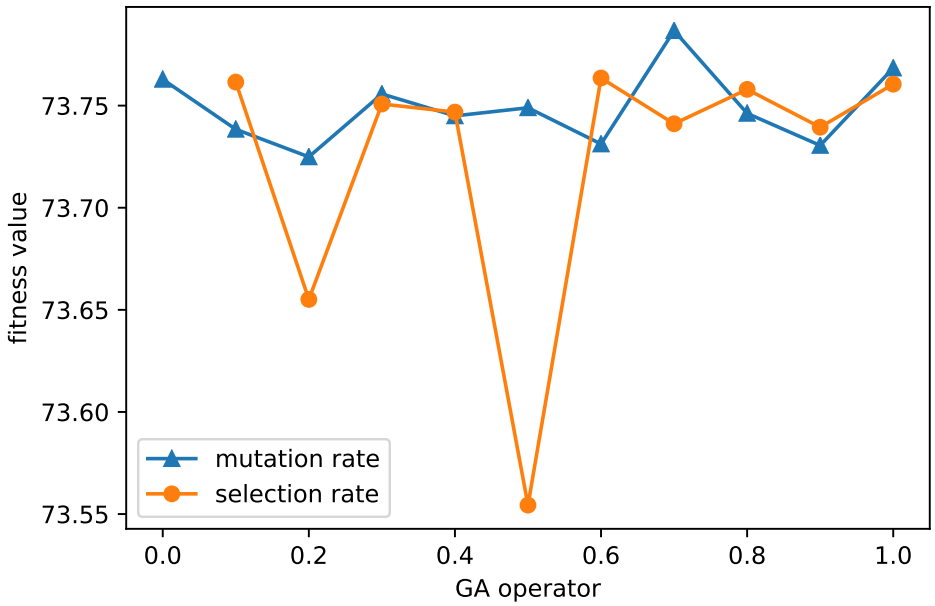

Figure 5.10: Fitness Vs. GA Operators

of objective function takes a dive and is thus, selected for the optimization. On the other hand, mutation rate is the probability at which 'genes' are modified to restore lost or unexplored region of search space. Although the suitable value of mutation rate is problem-specific, too high mutation rate renders the GA to be a pure random search routine which is not desirable [56]. For the present problem, the sensitivity analysis suggests that a probability of 0.2 is apt. Regardless, the value of the best-fitness is quite close for different rates of mutation as seen in Fig. 5.10. This can be attributed to the elitism strategy used in the routine that tends to preserve the optimum candidate at every generation.

5.3 Tests for various payload capacities

To qualitatively understand the effect of payload capacity on the body profile, a test run with four cases of different payloads is conducted. All the other set up parameters (except the gondola mass and payload) are kept identical to previous simulation to maintain comparability of the results. The gondola mass is measured to be 700 g with

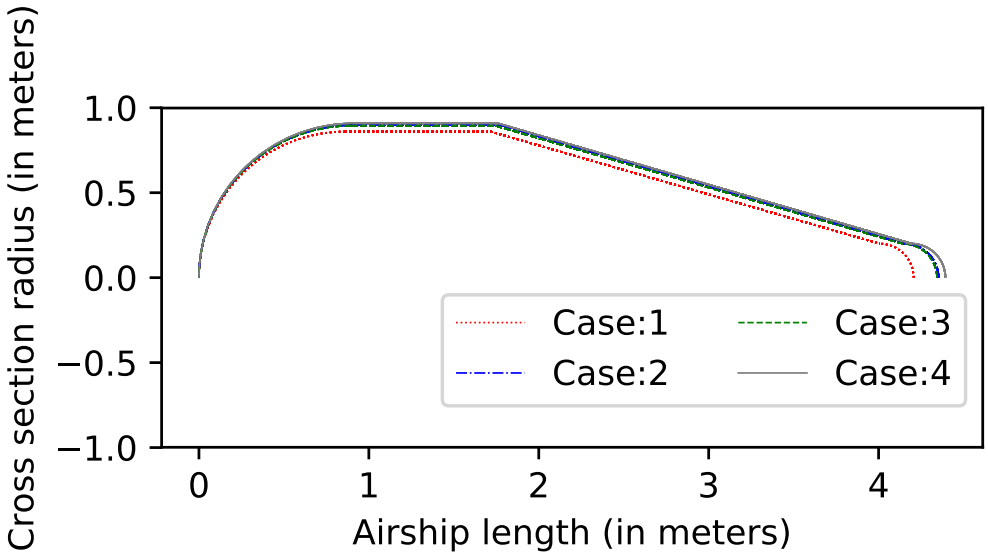

Figure 5.11: Simulation for various payload capacities

the fins weighing 32 g. The results obtained can be summarized as follows where the design vectors for the optimum solution is represented as vector x:

- Case 1: Payload 250 g

$$x = [0.8598 \quad 0.8568 \quad 2.29 \quad 0.2] \tag{5.9}$$

- Case 2: Payload 500 g

$$x = [0.8979 \quad 0.879 \quad 2.376 \quad 0.2] \tag{5.10}$$

- Case 3: Payload 750 g

$$x = [0.897954 \quad 0.850281 \quad 2.39844508 \quad 0.2] \tag{5.11}$$

Table 5.3: Comparison of characteristics for various payload configuration

Payload configuration (g)	Total mass(g)	Lifting gas volume (cu. m.)
250	4.71	6.02
500	4.95	6.2
750	5.2	6.312
1000	5.449	6.450

- Case 4: Payload 1000 g

$$x = [0.90755137 \qquad 0.851308 \qquad 2.434402 \qquad 0.20000193] \tag{5.12}$$

As can be seen in the Fig. 5.11, the variable 'c' is influenced the maximum for an increase in the payload capacity. On the other hand, the consistent dip in the value of 'd' is due to the prudent consideration of the aerodynamic consequence by the routine. Beyond the point of transition which occurs at the point of minimum pressure along the length of the airship, the wetted surface area has to be minimized in order to control the skin friction drag. Also, the shape vectors are obtained attained by eliminating certain possible optimization solutions that violate the lift density constraint for an unmanned airship development with neutral buoyancy. Another very important consideration: the size of the airship does not change by much for a 400% increase in payload. Therefore, larger airships are more effective. That being said, the trait is limited to a breakeven point after which the electronics design to steer the airship (power unit) becomes excessively larger to more than offset the buoyancy provided.

5.4 Confirmation to a commercial product

To establish the practical significance of the simulation output, several commercial and reported products are referenced in the section vis-à-vis the payload capacity, resource consumption and the airship efficiency.

5.4.1 Example 1

In Fig. 5.12, an off-the-shelf RC Zeppelin airship developed for advertising purposes available at Amazon.com is shown [57]. The height and the length of the airship are 1.5 m and 5 m respectively. It has a volume of 6.7 m^3 and a payload capacity of 1.2 kg. The vehicle can reach a maximum speed of 9.72 m/s. The HGA algorithm was simulated to decipher the volume requirement for the identical payload capacity

(a) Side view of RC airship (b) Bottom view of RC airship

Figure 5.12: Commercially available RC airship

with the present methodology. Consequently, the routine yielded a design vector as follows:

$$x = [0.900 \qquad 0.8560 \quad 2.407 \quad 0.200] \quad \text{in meters} \tag{5.13}$$

yielding the total length of 4.363 m with a total mass of 5.05 kg and the corresponding volume is 6.32 m^3. The mass of the keel assumed for the test is 100 g per unit length contributing a gross mass of 197 *grams* to the overall design. Evidently, for the identical payload configuration, the proposed design solution by the HGA has a lower resource consumption (volume or helium gas) and a superior aerodynamic characteristics due to its lower maximum radius. In conclusion, it can be said that the routine output is comparable to the commercial product in relation to the payload capacity.

5.4.2 Example 2

A similar attempt to size a semi-rigid airship for a selected shape (GNVR profile-elliptical, cylindrical, circular, parabolic) that is broadly along the same lines as the

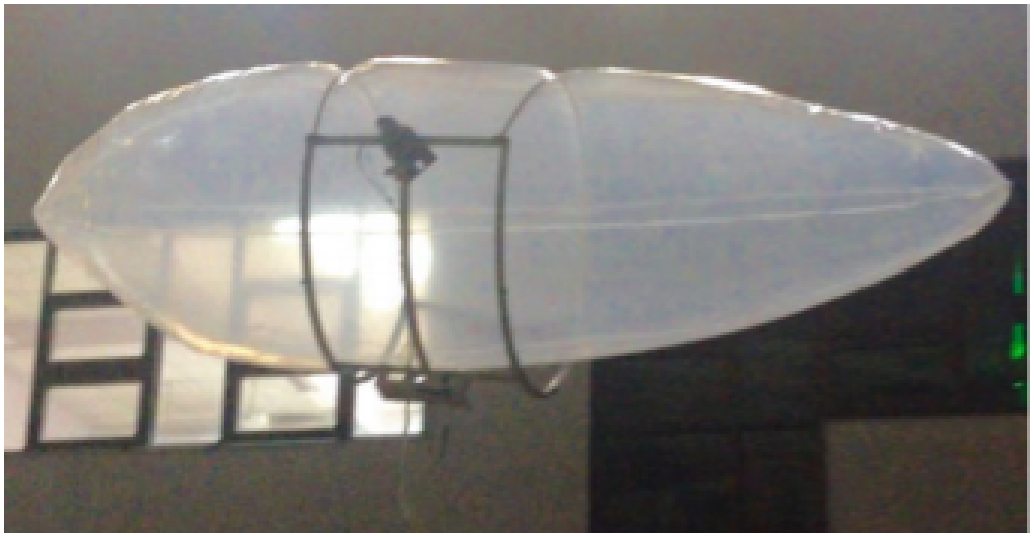

Figure 5.13: Simulation for various payload capacities [5]

present research is reported in the literature [5]. The fully assembled semi-rigid airship shown in Fig. 5.13 is chosen as a benchmark to compare the structural and flight parameters with the current work. The airship has a payload capacity of 400 g to be operated at ISA $+15^0$ conditions with an aim to achieve a portable structure for quick assembly [5] [58]. The lift ratio of the ship calculated using the empirical relation as follows:

$$LR = \frac{\text{All-up weight}}{\text{Payload capacity}} \tag{5.14}$$

is estimated to be 8.25 [5]. On the other hand, for an identical payload capacity, the present design is estimated to have an LR of 8.921. The airship is reported to be

Table 5.4: Comparison of different semi-rigid airships properties

Property	Literature [5]	Current design
Surface area (m^2)	14.08	14.9365
Envelope length (m)	4.305	4.25
Volume (m^3)	3.753	5.81
Maximum diameter (m)	1.311	0.8709
Mass of gondola (kg)	1.065	0.7
Drag coefficient (C_{DV})	0.0709	0.04720
Flight speed (m/s)	3	3.67

lighter owing to the absence of fins. However, like the present research, the airship shown in Fig. 5.13 is designed for neutral buoyancy with an oversized motor to generate extra upward thrust in case of an adverse weather condition. Furthermore, since the airship lacks fin structure, it is reported to experience inertial resistance to yaw movement. On the contrary, the present design is expected to be dynamically stable and controllable. The properties of the two designs are summarized in table 5.4. As can be noted, the algorithm output design has a larger volume, however, it offers a superior controllability and stability of the vehicle.

Chapter 6

Conclusion

6.1 Key findings

In this thesis, the airship helium envelope is optimized using hill-climbing genetic algorithm. An objective function was developed based on the design constraints of the semi-rigid unmanned airship with a sliding gondola. Furthermore, the methodology of optimization of the shape of the airship is based on payload and atmospheric conditions. Several previous works have considered hoop stress as one of the objective terms [15, 30, 24]. Unlike common practices, the airship used for the experiment is inflated slightly above atmospheric pressure and, hence, has negligible circumferential stresses. In the mathematical model of airship hull, the effects of uneven curve in shape due to a discontinuity at sphere and cylinder conjunctions i.e. between variables a, b; and c, d is neglected. As a result, the transition between each section is expected to be made smooth while manufacturing of the blimp in order to eliminate possible aerodynamic drag in the sharp points. The direct effects of fins in the surface area and center of gravity (CG) calculations are neglected. The fins could significantly affect the CG and the total area of the airship, e.g., the pitch angle at a certain gondola positions will be reduced. The aero-elastic effects are ignored in the present study considering the low flight velocity. An optimum design solution is obtained using the algorithm which is subsequently used to build an airship with the rapid descent ability. The algorithm was also simulated to obtain designs for a range of payload capacities i.e. 250 g to 1 kg. The present work provides a useful preliminary tool for optimization of airships. Due to inadequacy to express the overall drag as a function of geometry for complex geometries of airship hull, a post-optimization CFD tool can be used on a partially optimized shape. The proposed design is compared to other similar designs available commercially and in literature to correlate the significance of the results. The results indicate a good potential for the proposed approach to

optimize the airship for the mission requirements.

6.2 Future work

The current research could be extended to improve the model to take into account the continuous tail slope i.e. continuous transition from 'c' to 'd' as shown in Fig. 6.1. The CG of the fins could be modelled to make the design and estimation more precise. Along the same lines, a precise model of thrust and thrusters could be proposed. Researchers could work to predict the endurance and flight time of the airship to estimate the needs at design stage and optimize the overall design. Prospective researchers could extend the work to design for high-altitude missions for an enhanced range of payload capacity. The HGA results could be combined with a feed-forward

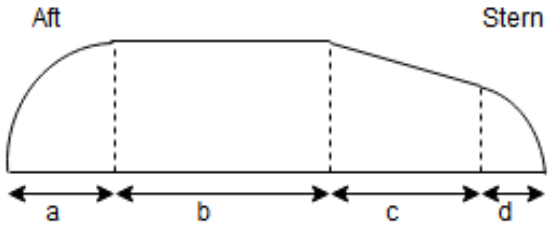

Figure 6.1: Airship body profile for future contributions

artificial neural network using back propagation to make the optimization process automatic [54]. The airship envelope is usually constructed by joining several smaller strips of the fabric [4]. Each such piece is termed as panel and a group of panels is referred to as a gore. Hence, further investigation in the gore design, for instance, using differential material construction that provides thick material at high stress areas and thin material at low stress regions of the hull, could be performed to enhance the overall efficiency of the airship [4].

References

[1] Gabriel Alexander Khoury. *Airship technology*, volume 10. Cambridge university press, 2012.

[2] Lin Liao and Igor Pasternak. A review of airship structural research and development. *Progress in Aerospace Sciences*, 45(4-5):83–96, 2009.

[3] Charles Blouin. *Trajectory optimization of a small airship*. PhD thesis, Université d'Ottawa/University of Ottawa, 2015.

[4] Amol Gawale, Amool Raina, Rajkumar Pant, and Yogendra Jahagirdar. Design, fabrication and operation of remotely controlled airships in india. In *The 26th Congress of ICAS and 8th AIAA ATIO*, page 8853, 2009.

[5] Sohrab R Mistr and Rajkumar S Pant. Design and fabrication of a quick dismantlable remotely controlled semirigid finless airship. In *Innovative Design and Development Practices in Aerospace and Automotive Engineering*, pages 103–116. Springer, 2017.

[6] Gabriel A Khoury and J David Gillett. Airship technology (cambridge aerospace series), 2004.

[7] Yasmina Bestaoui and Tarek Hamel. Dynamic modeling of small autonomous blimps. In *6th intern. conference on Methods and Models in Automation and Robotics, Miedzyzdroje*. Citeseer, 2000.

[8] Samuel Bueno, JosÃ© Azinheira, Josue Ramos, Ely Paiva, Patrick Rives, Alberto Elfes, JosÃ© R H Carvalho, and Geraldo F Silveira. Project aurora: Towards an autonomous robotic airship. 01 2002.

[9] The Lyncean Group of San Diego. Modern airships. https://lynceans.org/all-posts/modern-airships/, 2018.

[10] Augur RosAeroSystems. High altitude airship "berkut". http://rosaerosystems.com/projects/obj687, 2018.

[11] Eric Lanteigne, Wail Gueaieb, Dominic Robillard, and Steven Recoskie. Unmanned airship design with sliding ballast: Modeling and experimental validation. In *Unmanned Aircraft Systems (ICUAS), 2016 International Conference on*, pages 1246–1253. IEEE, 2016.

[12] Eric Lanteigne, Ahmad Alsayed, Dominic Robillard, and Steven G Recoskie. Modeling and control of an unmanned airship with sliding ballast. *Journal of Intelligent & Robotic Systems*, 88(2-4):285–297, 2017.

[13] Srikanth Saripalli, James F Montgomery, and Gaurav S Sukhatme. Visually guided landing of an unmanned aerial vehicle. *IEEE transactions on robotics and automation*, 19(3):371–380, 2003.

[14] Vahid Nejati and Kazuo Matsuuchi. Aerodynamics design and genetic algorithms for optimization of airship bodies. *JSME International Journal Series B Fluids and Thermal Engineering*, 46(4):610–617, 2003.

[15] Quan-bao Wang, Ji-an Chen, Gong-yi Fu, and Deng-ping Duan. An approach for shape optimization of stratosphere airships based on multidisciplinary design optimization. *Journal of Zhejiang University-SCIENCE A*, 10(11):1609–1616, 2009.

[16] Thorsten Lutz and S Wagner. Drag reduction and shape optimization of airship bodies. *Journal of Aircraft*, 35(3):345–351, 1998.

[17] Rajkumar Pant. A methodology for determination of baseline specifications of a non-rigid airship. In *AIAA's 3rd Annual Aviation Technology, Integration, and Operations (ATIO) Forum*, page 6830, 2003.

[18] Sasan Amani, Seid Hossein Pourtakdoust, and Farshad Pazooki. Multi-objective conceptual design optimization of a domestic unmanned airship. *Journal of Theoretical and Applied Mechanics*, 52, 2014.

[19] Joseph Mueller, M Paluszek, and Yiyuan Zhao. Development of an aerodynamic model and control law design for a high altitude airship. In *AIAA 3rd" Unmanned Unlimited" Technical Conference, Workshop and Exhibit*, page 6479, 2004.

[20] Sagar Kale, Pankaj Joshi, and Rajkumar Pant. A generic methodology for determination of drag coefficient of an aerostat envelope using cfd. In *AIAA 5th ATIO and16th Lighter-Than-Air Sys Tech. and Balloon Systems Conferences*, page 7442, 2005.

[21] Q Wang, J Chen, G Fu, D Duan, and H Zhao. A methodology for optimisation design and analysis of stratosphere airship. *The Aeronautical Journal*, 113(1146):533–540, 2009.

[22] C Vijay Ram and Rajkumar S Pant. Multidisciplinary shape optimization of aerostat envelopes. *Journal of aircraft*, 47(3):1073–1076, 2010.

[23] Haoquan Liang, Ming Zhu, Xiao Guo, and Zewei Zheng. Conceptual design optimization of high altitude airship in concurrent subspace optimization. In *50th AIAA aerospace sciences meeting including the new horizons forum and aerospace exposition*, page 1180, 2012.

[24] Xiao Zhang and Aiwu Zhang. Shape optimization of airship based on constrained particle swarm optimization. *JOURNAL OF INFORMATION &COMPUTATIONAL SCIENCE*, 10(18):5849–5857, 2013.

[25] Singiresu S Rao. *Engineering optimization: theory and practice*. John Wiley & Sons, 2009.

[26] Yogesh Jaluria. *Design and optimization of thermal systems*. CRC press, 2007.

[27] Kalyanmoy Deb and Mayank Goyal. Optimizing engineering designs using a combined genetic search. In *ICGA*, pages 521–528. Citeseer, 1997.

[28] Jasbir Arora. *Introduction to optimum design*. Elsevier, 2004.

[29] Randy L Haupt, Sue Ellen Haupt, and Sue Ellen Haupt. *Practical genetic algorithms*, volume 2. Wiley New York, 1998.

[30] Mohammad Irfan Alam, Shaik Subhani, and Rajkumar S Pant. Multidisciplinary shape optimization of stratospheric airships. In *International Conference on Theoretical, Applied, Computational and Experimental Mechanics (ICTACEM-2014)*, 2014.

[31] Christine M Anderson-Cook. Practical genetic algorithms, 2005.

[32] Christopher R Houck, Jeff Joines, and Michael G Kay. A genetic algorithm for function optimization: a matlab implementation. *Ncsu-ie tr*, 95(09):1–10, 1995.

[33] Manuel Lozano, Francisco Herrera, Natalio Krasnogor, and Daniel Molina. Real-coded memetic algorithms with crossover hill-climbing. *Evolutionary computation*, 12(3):273–302, 2004.

[34] Pablo Moscato et al. On evolution, search, optimization, genetic algorithms and martial arts: Towards memetic algorithms. *Caltech concurrent computation program, C3P Report*, 826:1989, 1989.

[35] Natalio Krasnogor and Jim Smith. Emergence of profitable search strategies based on a simple inheritance mechanism. In *Proceedings of the 3rd Annual Conference on Genetic and Evolutionary Computation*, pages 432–439. Morgan Kaufmann Publishers Inc., 2001.

[36] Ajith Abraham and Lakhmi Jain. Evolutionary multiobjective optimization. In *Evolutionary Multiobjective Optimization*, pages 1–6. Springer, 2005.

[37] Somayyeh Chamaani, Seyed Abdullah Mirtaheri, Mohammad Teshnehlab, and Mahdi Aliyari Shooredeli. Modified multi-objective particle swarm optimization for electromagnetic absorber design. In *Applied Electromagnetics, 2007. APACE 2007. Asia-Pacific Conference on*, pages 1–5. IEEE, 2007.

[38] Carlos A Coello Coello. Recent trends in evolutionary multiobjective optimization. In *Evolutionary multiobjective optimization*, pages 7–32. Springer, 2005.

[39] Yinjiang Li, Song Xiao, Paolo Di Barba, Mihai Rotaru, and Jan K. Sykulski. Localized probability of improvement for kriging based multi-objective optimization. 15, 12 2017.

[40] Jong Min Park, Bon Jun Ku, and Dae Sub Oh. Technical and regulatory studies on haps. In *GLOBECOM Workshops, 2008 IEEE*, pages 1–5. IEEE, 2008.

[41] Transport Canada. General operating and flight rules. https://www.tc.gc.ca/eng/civilaviation/regserv/cars/part6-standards-623d2-2450.htm, 2018.

[42] Transport Canada. Airworthiness manual. https://www.tc.gc.ca/eng/civilaviation/regserv/cars/part5-standards-541s-242.htm#541_15, 2018.

[43] Luftfahrt-Bundesamt. Transport airship requirements. https://www.faa.gov/aircraft/air_cert/design_approvals/airships/airships_regs/media/aceAirshipTARIssue1.pdf, 2000.

[44] Ralph D Lorenz. Flight power scaling of airplanes, airships, and helicopters: Application to planetary exploration. *Journal of Aircraft*, 38(2):208–214, 2001.

[45] Steven Recoskie, Eric Lanteigne, and Wail Gueaieb. A high-fidelity energy efficient path planner for unmanned airships. *Robotics*, 6(4):28, 2017.

[46] Antonio Dumas, Michele Trancossi, Mauro Madonia, Josè Pascoa, Galina Ilieva, and Agostino Coppola. Cfd analysis and optimization of a variable shape airship. In *ASME 2012 International Mechanical Engineering Congress and Exposition*, pages 161–166. American Society of Mechanical Engineers, 2012.

[47] Tushar Kanikdale, Anil Marathe, and Rajkumar Pant. Multi-disciplinary optimization of airship envelope shape. In *10th AIAA/ISSMO Multidisciplinary Analysis and Optimization Conference*, page 4411, 2004.

[48] Gu Zhengming. Research of stratospheric airships' skin material [j]. *Spacecraft Recovery & Remote Sensing*, 1:012, 2007.

[49] American Polyfilm. Polyurethane film products. =https://www.americanpolyfilm.com/products-main/, 2018.

[50] Keivan Borna and Vahid Haji Hashemi. An improved genetic algorithm with a local optimization strategy and an extra mutation level for solving traveling salesman problem. *arXiv preprint arXiv:1409.3078*, 2014.

[51] Jaya Shankar Tumuluru and Richard McCulloch. Application of hybrid genetic algorithm routine in optimizing food and bioengineering processes. *Foods*, 5(4):76, 2016.

[52] N Baskar, P Asokan, R Saravanan, and G Prabhaharan. Selection of optimal machining parameters for multi-tool milling operations using a memetic algorithm. *Journal of Materials processing technology*, 174(1-3):239–249, 2006.

[53] Cezary Z Janikow and Zbigniew Michalewicz. An experimental comparison of binary and floating point representations in genetic algorithms. In *ICGA*, pages 31–36, 1991.

[54] Pratibha Bajpai and Manoj Kumar. Genetic algorithm–an approach to solve global optimization problems. *Indian Journal of computer science and engineering*, 1(3):199–206, 2010.

[55] Wen-Yang Lin, Wen-Yung Lee, and Tzung-Pei Hong. Adapting crossover and mutation rates in genetic algorithms. *J. Inf. Sci. Eng.*, 19(5):889–903, 2003.

[56] Mandavilli Srinivas and Lalit M Patnaik. Adaptive probabilities of crossover and mutation in genetic algorithms. *IEEE Transactions on Systems, Man, and Cybernetics*, 24(4):656–667, 1994.

[57] Amazon. Air-ads 16ft 5 meter rc zeppelin outdoor radio control blimp advertising eblimp airship complete set, 2018.

[58] Sanyam S Mulay and Rajkumar S Pant. Design fabrication and flight testing of a non-rigid indoor airship. In *AIAA Lighter-Than-Air Systems Technology (LTA) Conference*, page 1297, 2013.

[59] Stephen Boyd and Lieven Vandenberghe. *Convex optimization*. Cambridge university press, 2004.

Appendix A

Appendix: Important concepts

Convex optimization and convex set

Convex optimization is often seen as a mixture of three disciplines: convex analysis, numerical computation, and optimization [59]. Let S be a convex set, that is, a region in the n-dimensional space satisfying the convexity condition, that is, for any two points in the set, the line passing through them is also in S. Then, the convexity of a function can be formally defined as, for a function f_i of n variables to be convex on a convex set S, it must satisfy the inequality condition for any two points $\mathbf{x}$ and $\mathbf{y}$ in S as follows [59]:

$$f_i(\alpha\mathbf{x} + \beta\mathbf{y}) \leq \alpha f_i(\mathbf{x}) + \beta f_i(\mathbf{y}) \tag{A.1}$$

if $\alpha+\beta = 1, \quad \alpha \geq 0, \beta \geq 0$, where α and β are any arbitrary positive scalars while $\mathbf{x}$ and $\mathbf{y}$ are n-dimensional vectors in the space. Also, a set is said to be affine if always, a line through any two distinct points x_1, x_2 in the set could be obtained such that:

$$x = \theta x_1 + (1 - \theta x_2) \qquad (\theta \epsilon \mathbf{R}) \tag{A.2}$$

For example, a solution set of linear equations $x|Ax = b$ is an affine set. In comparison, the convex set is a special case of affine set so that the value of θ is always positive for a convex set. Some of the common engineering convex optimization problems encountered in the literature are: multi-period processor speed scheduling, minimum time optimal control, grasp force optimization etc [59].

The ability to understand a problem to be a convex problem is a blessing in the sense that it enables us to optimize a larger class of problems. A majority of which belong to constrained optimization problem of the form [59]:

$$\text{minimize} \quad f_0(x) \tag{A.3}$$

$$\text{subject to} \quad f_i(x) \leq 0, \qquad i = 1, 2, ..., m \tag{A.4}$$

$$h_i(x) = 0, \qquad i = 1, 2, ..., p \tag{A.5}$$

where, the function f_0 is the cost function, f_i is the set of inequality constraint, h_i is the set of equality constraint. To put into perspective the importance of convexity of a problem, if all the f_i constraints are convex, and the h_is are affine, then any local optimum is also the global optimum i.e. no local minimum traps, and therefore, such problems can be efficiently solved by polynomial time complexity algorithms and so on [28].